Science of the Total Environment 948 (2024) 174697

Contents lists available at ScienceDirect

Science of the Total Environment

journal homepage: www.elsevier.com/locate/scitotenv

The fate of post-use biodegradable PBAT-based mulch films buried in agricultural soil

Fabiana Convertino [a,1], Sabrina Carola Carroccio [b,1], Maria Cristina Cocca [c], Sandro Dattilo [b], Anna Chiara Dell'Acqua [a], Luca Gargiulo [c], Luca Nizzetto [d,e], Paolo Maria Riccobene [b], Evelia Schettini [a,*], Giuliano Vox [a], Domenico Zannini [f], Pierfrancesco Cerruti [c]

[a] Department of Soil, Plant and Food Science, University of Bari, Bari, Italy
[b] National Research Council of Italy, Institute of Polymers, Composites and Biomaterials (CNR-IPCB), Catania, Italy
[c] National Research Council of Italy, Institute of Polymers, Composites and Biomaterials (CNR-IPCB), Pozzuoli (Naples), Italy
[d] Norwegian Institute for Water Research, Oslo, Norway
[e] Research Centre for Toxic Compounds in the Environment, Masaryk University, Brno, Czech Republic
[f] National Research Council of Italy, Institute of Chemical Sciences and Technologies "G. Natta" (CNR-SCITEC), Genova, Italy

Abbreviations: A/T, adipate-to-terephthalate ratio; BIO-0, pristine biodegradable mulch film; BIO-0-*number, pristine biodegradable mulch film after *number days of burial; BIO-A192, artificial aged biodegradable mulch film; BIO-A192-*number, artificial aged biodegradable mulch film after *number days of burial; $CHCl_3$, chloroform; ΔHm, melting enthalpy; DSC, differential scanning calorimetry; DTG, differential thermograms; EB, elongation at break; FTIR, Fourier transform infra-red; GC, gas–chromatography; GPC, gel permeation chromatography; HABA, 2-(4-Hydroxyphenylazo)benzoic acid; ICP-MS, inductively coupled plasma mass spectrometry; LWIR, long wave infra-red; m/z, mass/charge; MALDI-TOF, matrix-assisted laser desorption/ionization time-of-flight mass spectrometry; MF, mulch film; MM, molar mass; MS, mass spectrometry; M_w, molecular weight; PAR, photosynthetically active radiation; PBAT, poly(butylene-adipate-*co*-terephthalate); PLA, polylactic acid; PE, polyethylene; Py-GC–MS, pyrolyzer/gas–chromatography mass spectrometry; RCS, refrigerated cooling system; RT, retention time; SEM, scanning electron microscope; sBIO-0, BIO-0 solubilised in $CHCl_3$; sBIO-A192, BIO-A192 solubilised in $CHCl_3$; SOIL-BIO-0, soil in which BIO-0 film was buried, taken at the end of the experimental test; SOIL-BIO-A192, soil in which BIO-A192 film was buried, taken at the end of the experimental test; SOIL-0, control soil sample, soil without buried films; sSOIL-BIO-0, BIO-0 components extracted in $CHCl_3$ from SOIL-BIO-0; sSOIL-BIO-A192, BIO-A192 components extracted in $CHCl_3$ from SOIL-BIO-A192; TD, thermal desorption; TG, thermogravimetry; THF, tetrahydrofuran; TS, tensile strength; UV radiation, ultra violet radiation; WAC, water contact angle; WL, weight loss.

* Corresponding author.
E-mail address: evelia.schettini@uniba.it (E. Schettini).

[1] Equal first authors: Fabiana Convertino and Sabrina Carola Carroccio have contributed equally.

https://doi.org/10.1016/j.scitotenv.2024.174697

Available online 15 July 2024

HIGHLIGHTS

- In-field burial tests of starch/polyester mulch films carried out for 478 days.
- Surface of mulch film decreases by 57 %, and microplastics are found in soil.
- Complex composition of biodegradable mulch films influences degradation behaviour.
- Photooxidation of mulch films reduces polyester degradability due to crosslinking.
- Burial results in an enrichment of terephthalic units in mulch film.

GRAPHICAL ABSTRACT

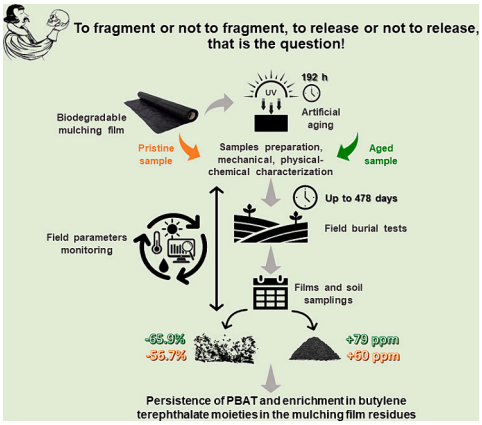

ARTICLE INFO

Keywords:
Biodegradable microplastics
In-field degradation
Plastic residues pollution
Environmental impacts
MALDI investigation
Pyrolysis GC/MS identification

ABSTRACT

The fate of black biodegradable mulch film (MF) based on starch and poly(butylene-adipate-*co*-terephthalate) (PBAT) in agricultural soil is investigated herein. Pristine (BIO-0) and UV-aged film samples (BIO-A192) were buried for 16 months at an experimental field in southern Italy. Visual, physical, chemical, morphological, and mechanical analyses were carried out before and after samples burial. Film residues in the form of macro- and microplastics in soil were analyzed at the end of the trial.

Progressive deterioration of both pristine and UV-aged samples, with surface loss and alterations in mechanical properties, occurred from 42 days of burial. After 478 days, the apparent surface of BIO-0 and BIO-A192 films decreased by 57 % and 66 %, respectively. Burial determined a rapid depletion of starch from the polymeric blend, especially for the BIO-A192, while the degradation of the polyester phase was slower. Upon burial, an enrichment of aromatic moieties of PBAT in the film residues was observed, as well as microplastics release to soil. The analysis of the MF degradation products extracted from soil (0.006–0.008 % by mass in the soil samples) revealed the predominant presence of adipate moieties. After 478 days of burial, about 23 % and 17 % of the initial amount of BIO-0 and BIO-A192, respectively, were extracted from the soil. This comprehensive study underscores the complexity of biodegradation phenomena that involve the new generation of mulch films in the field. The different biodegradability of the polymeric components, the climate, and the soil conditions that did not strictly meet the parameters required for the standard test method devised for MFs, have significantly influenced their degradation rate. This finding further emphasizes the importance of implementing field experiments to accurately assess the real effects of biodegradable MFs on soil health and overall agroecosystem sustainability.

1. Introduction

Plastic pollution in the atmosphere, soil, and water represents an important present-day environmental issue (Li et al., 2023; Zhou et al., 2023; Qi et al., 2023). Most of the research carried out so far has been mainly focused on microplastic pollution in marine and aquatic ecosystems (Kim et al., 2021). Nowadays, there is an increasing interest in plastic pollution in terrestrial ecosystems due to the pressure posed to plant-soil health, animals, and humans (Ng et al., 2018). In this frame, agricultural plastic mulch films (MFs) have been recognized as an important source of microplastics entering agricultural soil (Qiang et al., 2023). Plastic MFs have several positive effects, for example, reducing water evaporation from the soil, weed growth, and soil erosion. On the other hand, a plastic MF can generate microplastics depending on chemical composition, film type, aging in the field, and agricultural practices performed such as tillage (Qi et al., 2023). Also, climatic and environmental conditions, such as ultraviolet (UV) irradiation, temperature of air and soil, and wind, can induce fragmentation of the plastic material into smaller particles (Liu et al., 2023). Several authors (Qiang et al., 2023; Kim et al., 2021; Serrano-Ruiz et al., 2021) reported the presence of polyethylene (PE) microplastics in agricultural soil environment, indicating that microplastic contamination may mainly derive from commonly used PE MFs. The constant use of PE mulches causes plastic fragments and chemicals to accumulate year after year in agricultural soils, compromising soil health, food security, and environmental sustainability (Serrano-Ruiz et al., 2021; Fan et al., 2023).

Research centers and industries are being actively involved in the development of biodegradable films for mulching applications to achieve behaviour, functionality, and agronomic performance like those of conventional plastic films, while offering an option for farmers to avoid dealing with the problem of waste from conventional MFs. To this aim, biodegradable MFs have been developed, made of blends of natural polymers (e.g., starch) and synthetic polyesters, which also contain a range of additives to improve their properties.

Biodegradation in soil is generally assessed by laboratory respirometric tests able to measure CO_2 production at a constant temperature between 20 °C and 28 °C, in accordance with the ASTM D 5988e18 or ISO 17556 test methods (Tosin et al., 2020; Degli Innocenti et al., 2022; Chinaglia et al., 2024). A mineralization percentage threshold of 90 % (absolute or relative to the reference material) in a laboratory test period of up to 24 months is considered an indicator of total biodegradation and lack of remaining chemical residues (Tosin et al., 2020). However,

laboratory tests are performed under constant moisture and temperature conditions, while remarkable seasonal changes in soil temperature and moisture characterize in-field conditions. Consequently, the standard method adopted in the laboratory test does not fully guarantee the reproduction of a real case of materials biodegradation (Griffin-LaHue et al., 2022).

A suitable biodegradable MF in contact with soil should undergo a biodegradation process that finally leads to its complete macroscopical and microscopical disappearance, whereby, during such degradation, its residues do not negatively affect soil health. However, biodegradable MFs comprise a mix of chemicals, including fillers, additives, and polymers, characterized by different biodegradability rate and extent. As a result, residues of non- or slowly biodegradable substances could persist in the soil (or be transported to water or atmosphere) at a micro and nanoparticle scale or as low molecular weight compounds (e.g. in the case of chemical additives with a longer persistence than the polymeric matrix) (Zhang et al., 2024). The effect of such residues and the associated possible pollution derived from microplastics on soil remains uncertain, and it is still largely unknown how these compounds interact once broken down (Serrano-Ruiz et al., 2021; Huang et al., 2023). Biodegradable mulches will undergo fragmentation, and fragment accumulation may have some effects as found for PE (Zhang et al., 2024). To overcome this literature gap, more studies are required to assess in-situ degradation in different climate areas and over long temporal periods. Since the degradation process is influenced by the characteristics of soil, as well as the climatic and environmental conditions, such as microbial community, temperature, and moisture content (Sintim et al., 2020; Huang et al., 2023), there are several uncertainties regarding the long-term impacts on human and plant-soil health, and ecosystem multifunctionality in agroecosystems (Zhou et al., 2023; Serrano-Ruiz et al., 2021; Huang et al., 2023).

Based on these considerations, the aim of this paper is to investigate the fate of a biodegradable MF in agricultural soil by evaluating nature and quantity of both macroscopic film residues and related microplastics released from the film after burial through chemical-physical, structural, and mechanical characterization. Pristine and artificially aged films, which simulate the behaviour of the material during and after use, respectively, were buried for 16 months in the field in Mediterranean climate conditions. This investigation aims to gain insight into the degradation over time of biodegradable films under real conditions, providing new data useful to refine their formulation for safe use in agriculture.

2. Materials and methods

2.1. Tested materials

A roll of a 0.015 mm-thick black biodegradable film for soil mulching (coded as BIO-0) complying with the EN 17033 European standard was purchased from a local supplier. To avoid any bias due to knowledge of material and film composition, the authors decided to buy the film in a blind way.

From BIO-0 film, specimens of 8.2 cm × 32.2 cm were cut and artificially aged by thermal and UV-light irradiation. Aging was performed by a Q Lab accelerated chamber equipped with UVA lamps with a maximum emission at 340 nm. The irradiance at the wavelength peak was set at 0.68 W/m^2/nm at 60 °C. Film specimens were irradiated for 192 h (coded as BIO-A192), which corresponds to 850 MJm^{-2} of exposure to solar radiation in an open field (Escobedo et al., 2009), approximately 2 spring months in Southern Italy. Then, pristine and irradiated film specimens were subjected to planned analyses and burial tests.

BIO-0 and BIO-A192 were buried at the experimental field of the University of Bari and withdrawn after different time intervals. Laboratory tests were carried out on film specimens before burial in the experimental field and at different burial time intervals.

Solvents, tetrahydrofuran (THF) and chloroform ($CHCl_3$), and 2-(4-hydroxyphenylazo)benzoic acid (HABA) matrix for mass spectrometry analysis, were purchased from Sigma Aldrich (Merck Spa, Milan, Italy).

2.2. Laboratory tests

2.2.1. Gel permeation chromatography

The molar masses (MMs) and their distribution were measured using a Knauer AZURA® SEC Lab system in THF anhydrous solution at 40 °C (≥99.9 %, for gel permeation chromatography (GPC), stabilized with 250 ppm of butylated hydroxytoluene as inhibitor). The flow rate was set at 0.6 mL/min using an AZURA P 6.1 L isocratic pump system with four TSK gel Super columns in series (H2500, H3000, H4000, and H5000, respectively), and an AZURA RID 2.1 L refractive index detector. A volume of 50 μL of THF sample solution at a concentration of 2.0 mg/mL was injected into the system using an AZURA AS 6.1 L autosampler. Polystyrene standards were used to build up the calibration curve.

2.2.2. Mass spectrometry characterization

To identify the nature of the polymeric matrices constituting the MF, Thermal Desorption (TD) or pyrolyzer/gas–chromatography Mass Spectrometry (Py-GC–MS) and Matrix-Assisted Laser Desorption/Ionization Time-of-Flight MS (MALDI-TOF) analyses were performed. A 4800 MALDI TOF/TOF™ analyzer (Applied Biosystems, Framingham, MA, USA) was used to acquire MALDI-TOF spectra. The instrument was equipped with a Nd:YAG laser with 355 nm wavelength of <500 ps pulse and 200 Hz repetition rate. MALDI-TOF mass spectra were recorded in reflectron and positive ion mode. HABA (0.1 M in $CHCl_3$/THF 20:80) was used as a matrix. The MF was treated with $CHCl_3$, and the soluble polymer fraction was filtered and concentrated. Appropriate polymer and matrix solution *v*olumes were mixed to obtain 2:1, 1:1, and 1:2 ratios (sample/matrix *v*/v). 1 mL of each sample/matrix mixture was spotted on the MALDI-TOF sample holder and slowly dried to allow matrix crystallization. At least three separate film portions were analyzed. The resolution of the MALDI-TOF spectra reported in the text is about 7000–8000 FWHM, and the accuracy of mass determination ranges from 19 to 30 ppm in the mass range of 1000–3000 Da.

TD, Py-GC–MS analyses were carried out on 0.1 mg of film sample. Pyrolysis was performed in a Multi-Shot Pyrolyzer (EGA/PY-3030D, Frontier Labs), connected to a GC system GC-2020 (Shimadzu Corporation), coupled with triple quadrupole MS detector and electronic ionization (70 eV) Mass Detector TQ8040 (Shimadzu Corporation). The GC instrument was equipped with Ultra Alloy® Metal Capillary Column (Frontier Labs, stationary phase 5 % di-phenyl-methyl poly siloxane, with an inner diameter of 250 μm, a film thickness of 0.25 μm and a length of 30 m). Interfaces of Py-GC and GC–MS were kept at 300 °C and 250 °C, respectively. To simplify the chromatogram, three steps in temperature were performed to analyze the sample. Specifically, the analyses were carried out at 300 °C and 400 °C. The GC oven temperature was held at 50 °C for 1 min, increased to 100 °C at 30 °C/min, then held at 100 °C for 5 min, from 100 °C to 300 °C at 10 °C/min, and finally, it was stabilized at 300 °C for 10 min. Helium was used as carrier gas at a controlled flow of 1.78 mL/min. The split ratio was 1/50 of the total flux. Blanks were performed before each measurement by placing an empty crucible in the furnace and performing pyrolysis in the same conditions mentioned above. Chemical structures were determined by matching experimental spectra with those collected in the MS libraries (NIST11.Lib.; NIST11s.Lib.; WILEY8.LIB).

Inductively coupled plasma mass spectrometry (ICP-MS). Film samples were mineralized with an Anton-Paar Multiwave 3000 Microwave digestion system in polytetrafluoroethylene vessels. Then, according to EPA Method 3052, 3.5 mL of HNO_3 and 1.5 mL of H_2O_2 were added to the digestion mixture. After that, the content of vessel was diluted with 5 mL of water and filtered using Whatman 40 filters. An aliquot of 1 mL, taken from the filtrate, was diluted to 50 mL and then subjected to the ICP-MS analysis by using a Perkin Elmer ICP-MS model

Nexion 300× (Perkin Elmer Inc. Waltham, MA, USA) device, according to EPA Method 6020. The results were normalized with blanks of mineralization (which includes filtration) and measurement, so the values are reported in mg/kg. Each determination was performed three times.

2.2.3. Thermal properties

Thermogravimetry (TG) measurements were performed using a Perkin Elmer Pyris 1 thermo-balance (Perkin Elmer, Milan, Italy). An amount of 4.5 ± 0.5 mg of sample was placed in open crucibles and heated from 25 °C to 650 °C at a 10 °C/min rate. The tests were performed in an inert atmosphere with a 40 mL/min nitrogen flow rate. Differential scanning calorimetry (DSC) on MFs was carried out by using a Q2000 T_{zero} differential scanning calorimeter (TA Instrument, New Castle, DE, USA), equipped with a Refrigerated Cooling System (RCS) accessory for fast cooling. The calorimeter was calibrated in temperature and energy using indium. Dry nitrogen was used as purge gas at a rate of 30 mL/min. DSC measurements of the film samples were performed in a double heating run; the first one, from 20 °C to 200 °C, at 20 °C/min, was followed by an isothermal step of 1 min and a cooling step from 200 °C to -80 °C at a rate of 20 °C/min. Afterward, an isothermal step of 1 min and, finally, a second heating ramp up to 250 °C at 20 °C/min were performed.

2.2.4. Mechanical characterization

The tensile properties of the MFs were measured by an Instron series 4505 dynamometer at 23 ± 1 °C and 50 % RH. The sample thickness was measured using a digital micrometer (IP65 Mitutoyo, Kawasaki, Japan), and the tensile data were reported as average value of three different measurements. The tensile properties of the films were measured in accordance with ISO 527-1:2019 standard test.

2.2.5. Morphological analysis: Scanning electron microscopy

Morphological analysis of the film surfaces was performed by means of a Quanta 200 FEG scanning electron microscope (SEM) (FEI, Eindhoven, The Netherlands). Film surfaces were coated with a homogeneous layer (18 ± 0.2 nm) of Au and Pd alloy by means of a sputtering device (MED 020, Bal-Tec AG, Tucson, AZ, USA). The micrographs were taken at room temperature, in high vacuum mode.

2.2.6. Film wettability: Water contact angle and swelling ratio tests

Before testing, the samples were subjected to different washing cycles to eliminate the residues of soil firmly attached to their surface after burial. The samples were repeatedly immersed in 20 mL of deionized water, then blotted with absorbent paper, until no soil residues were spotted on the paper. Before testing, the samples were then dried in an oven at 40 °C for 24 h. Water contact angle (WCA) measurements were performed by a First Ten Angstroms FTA1000 instrument (Portsmouth, VA, USA), equipped with a high-resolution video camera (752 × 582 pixels, image acquisition speed of 25 frames per second), and the data were analyzed by KRUSS software (RTA 32). The static WCA (θ, deg) was measured at room temperature by a sessile drop method by dispensing 2 μL drops of distilled water onto the film surface using an automatic pipette. The droplet was released from 0.5 cm above the polymer surface to ensure consistency of the measurements. The WCA was calculated immediately after droplet deposition as the angle between the baseline of the drop and the tangent. For each sample, 5 WCA measurements were taken and averaged. The detections were performed at a stabilized condition of 25 °C and 50 wt% relative humidity.

To calculate swelling, a square strip of MF sample (1 cm × 1 cm) was weighed at zero time (m_1) and immersed into 20 mL deionized water for different times (0, 1, 2, 3, and 5 h). The residual water on the sample surface was carefully wiped off, and the sample was then weighed (m_2). The swelling ratio was calculated using the following equation:

$$Swelling\ ratio\ (\%) = \frac{m_2 - m_1}{m_1} * 100 \quad (1)$$

2.2.7. Radiometric characterization

Radiometric laboratory tests were performed on BIO-0 and BIO-A192 MFs before burial at the experimental field.

Spectral direct transmissivity of the films in the solar wavelength range, from 200 nm to 2500 nm, was measured by a double beam UV-VIS-NIR spectrophotometer (Lambda 950, Perkin Elmer Instruments, Norwalk, CT, USA). Measurements were performed in steps of 10 nm using radiation with a direct perpendicular incidence. Spectral total and diffuse transmissivity and reflectivity were measured by means of an integrating sphere (diameter 100 mm) used as receiver of the spectrophotometer, with a double beam comparative method. The spectral transmissivity and reflectivity in the long wave infra-red (LWIR) range, between 2500 nm and 25,000 nm, were measured by a FT-IR spectrophotometer (1760 X, Perkin Elmer Instruments, Norwalk, CT, USA) in steps of 4 cm^{-1}. Spectral transmissivity was measured using radiation with a direct perpendicular incidence; reflectivity was measured at near normal incidence (10°).

The transmissivity and reflectivity tests were performed on five samples (40 mm × 40 mm) both in the solar and in the LWIR range. The radiometric coefficients in the solar wavelength range (200–2500 nm) and in the photosynthetically active radiation (PAR) range (400–700 nm) were calculated as the weighted average value of the spectral transmissivity using the spectral distribution of the solar radiation at ground level as a weighting function (Vox et al., 2005; Schettini and Vox, 2012). The transmissivity coefficients in the LWIR range were calculated as average values of the spectral transmissivity in the wavelength range from 7500 nm to 12,500 nm.

2.3. Experimental design and location

The field test was carried out at the experimental farm of the University of Bari, in Valenzano (Bari, Southern Italy). Latitude, longitude, and elevation of the site are 41° 01′ N, 16° 54′ E, and 124 m a.s.l., respectively. The area is characterized by a Mediterranean climate, mild temperate with humid and hot summer, defined as Cfa by Köppen-Geiger climate classification (Kottek et al., 2006). The soil has a sandy clay loam texture (54.31 % sand, 17.62 % silt, and 28.07 % clay), characterized by a pH in H_2O equal to 8.09, an organic carbon content equal to 17.52 g/kg of the fine earth (**Table S1**). The experimental field test lasted 478 days, from June 7, 2022, to September 28, 2023.

The experimental area was a rectangle of about 80 m^2, divided into smaller rectangles each with dimensions of 0.50 m × 0.80 m (**Fig. S1**). Each rectangle was identified with a capital letter indicating the line and a number indicating the column. Inside each rectangle, three samples of the same material were buried and identified with a lowercase letter.

Specimen preparation and burial were performed similarly for both pristine and artificially aged materials.

Before the burial, each specimen was cut, labeled, and measured (thickness, dimension, weight). Film specimens had a mean dimension of 10 cm × 20 cm. Film thickness was measured using a micrometer. A precision balance with a maximum capacity of 200 g and 0.001 g accuracy (WTC 200 Precision Balance, RADWAG, Poland) was used to weigh the specimens. For the thickness and the weight, 5 measurements were performed, and the mean was reported. The BIO-0 and BIO-A192 specimens were characterized by mean weight and thickness of 0.341 g and 11.14 μm, and 0.343 g and 12.36 μm, respectively. After characterization, digital images of each specimen were taken.

Data loggers and sensors were used to monitor climatic and soil parameters in the field. Air temperature and relative humidity were measured by HygroClip-S3 sensors (Rotronic, Zurich, Switzerland), wind speed, and direction by means of a Wind Sentry anemometer (model 03002, R.M. Young Company, USA). Solar radiation on the

horizontal plane was measured by means of a pyranometer (model 8–48, Eppley Laboratory, Newport, RI, USA). Rain was monitored over time from the beginning of the test (ARIF, 2024). Soil temperature and water content sensors were placed at three different field points 10 cm deep. Soil temperature and water content were measured by means of RT-1 sensors (METER Group, Inc., Pullman, WA, USA) and ECH2O 10HS sensors (METER Group, Inc., Pullman, WA, USA), respectively. The recording of the measurements started in June 2022 for the external environmental parameters and in July 2022 for the soil parameters. Measures were taken every 60 s, averaged every 15 min, and stored in the data logger.

Monthly mean values of the external air temperature recorded during the test period are summarized in **Table S2**. The period from June 2022 to September 2023 was characterized by monthly maximum values of the external air temperature ranging from 18.7 °C (recorded in February 2023) to 45.3 °C (recorded in July 2023) and by monthly minimum values of external air temperature ranging from 0.9 °C (recorded in February 2023) to 18.4 °C (recorded in August 2023).

Before starting the field test, laboratory analyses were carried out on soil samples taken from different spots in the field. The soil properties evaluated in June 2022 are shown in **Table S1**.

The burial operations took place on 7 June 2022, burying the specimens 10 cm deep. Each specimen was embedded in a natural white high-density PE net (mesh of 2.7 mm × 7 mm; thread diameter of 0.29 mm) and then buried in the soil. The net was needed to collect the MF samples subjected to the burial tests. The selected net's mesh did not prevent organisms from passing through, allowing the MF to degrade similarly without it. External labels were applied to identify the specimens.

No plant cultivation was carried out during the test; weeds were cut periodically with a brush cutter.

An automatic irrigation system was set up. Only during summertime watering was planned for 90 min, at 2.00 am once a week. About 30 L per square meter of water were provided.

The unearthing procedure for collecting both types of MF specimens from the field was the following. Three specimens of both MFs were collected from three different rectangles, randomly chosen in the field, each located far from each other. During the retrieval operation, the 10 cm of soil covering the specimen was carefully removed by hand. Once the above soil was removed, the film specimen was carefully taken. Even if irrigation was stopped some days before collection, the soil could not be completely dry, and specimens were dirty with soil. As the weeks passed, small weed roots were sometimes found on the film specimens. To remove soil from the specimens, each specimen was gently dusted both with a breath of air and using an artist's brush with soft bristles. The specimens which were not too much degraded were carefully and gently washed to remove the soil. The washing water was poured into the soil at the point where the specimen was taken; thus, residues were not dispersed but added to the soil. After washing, the specimens were left to dry to be used for subsequent measurements and analyses.

The unearthed specimens were coded adding a number indicating the days of burial in the field; for example, BIO-A192–241 refers to a specimen that was artificially aged for 192 h and buried in the field for 241 days.

For accurate visual analysis of the degradation status of the collected film specimens, photos and scanned images were taken. Photos were taken in the field; color, grayscale, and black/white images for both sides of each specimen were acquired by the scanner.

The availability of each specimen's pictures before and after the burial was useful for their comparison by performing digital image analyses based on the pixel recognition technique. To this aim, the free graphic software GIMP (GNU Image Manipulation Program, https://www.gimp.org) was used. The surface of an A4 sheet was used as a calibration area. Based on the pixel and the surface in cm^2 of the calibration area, the specimen's surface pixels were correlated to the calibration area to obtain the specimen's surface in cm^2. Then, the specimen areas before and after burial were compared; the procedure was repeated for each specimen.

At the end of the experimental test, 478 days after the burial, soil samples (coded as SOIL-BIO-0 and SOIL-BIO-A192) were taken to evaluate the presence of microplastics due to the burial of the materials. An approximately 5 cm thick soil layer underneath the MF was taken as a soil sample, weighing about 1000 g. In an area without buried specimens, at a depth of 10 cm, a layer about 5 cm thick of soil was taken as control and coded as SOIL-0.

2.4. Characterization of the microplastics released from MF to soil and the MF degradation products in soil

Extraction of microplastics for qualitative analysis. In order to isolate microplastics, possibly released from MF to soil, 50 g of soil, for each sample, was mixed with 25 mL of canola oil and 375 mL of distilled water in glass-necked flasks equipped with removable glass caps. The flasks were capped and vigorously shaken to homogenize the sample. After that, they were left to stand for 24 h to settle. Shaking and sedimentation were repeated three times to allow the oil to intimately contact the soil and plastic particles present in the soil sample. The oil phase was removed and filtered through an 8 μm pore-size cellulose nitrate filter (Sartorius Stedim Biotech, Gottingen, Germany). Additionally, ethanol (96 %) and hot water were used to clean the filter during filtration to remove oil traces. To recover microparticles from filter surfaces, filters were immersed in 10 mL of distilled water and sonicated using an ultrasonic bath at 40 kHz for 30 min. The obtained dispersions were filtered through a 5 μm pore-size silicon filter (MakroPor, Thermo Fisher Scientific). Finally, filters were washed with ethanol and dried at room temperature for 24 h.

Chemical identification. Silicon filters were analyzed using a Fourier transform infra-red (FTIR) micro spectrometer Nicolet iMX10 (Thermo Fisher Scientific). FTIR spectra were acquired using 64 scans and 4 cm^{-1} resolution in the range 4000–650 cm^{-1} using an aperture size of 50 μm × 50 μm.

Quantification of the MF degradation products in soil. For the quantitative analysis of MF residues in soil, the latter was subject to solvent extraction to dissolve the MF degradation products released upon burial. To this aim, 200 g of soil was mixed with 300 mL of $CHCl_3$ and stirred overnight with an orbital shaker at room temperature at 300 rpm. The solution was recovered and concentrated by vacuum distillation with a rotary evaporator, until a volume of 4 mL. Then, TG was used to further concentrate it using the Perkin Elmer Pyris 1 analyzer. To this purpose, 100 μL of each solution was placed in a platinum open pan, and high-purity nitrogen was fluxed through the furnace at a flow rate of 40 mL/min at 70 °C for about 20 min to remove the solvent. After weight equilibration, the sample was then heated from 70 °C to 650 °C at 10 °C/min. FTIR analysis was performed on the dissolved components after casting the solutions on KBr disks. For comparison, a known amount of BIO-0 and BIO-A192 was dissolved in 4 mL of $CHCl_3$ and analyzed by TGA and FTIR using the same procedure.

2.5. Statistical analysis

One-way ANOVA test was performed using OriginPro 8.5 software, to assess significant differences (significance level $p < 0.05$) in mean values of buried films (both pristine and artificially aged samples).

2.6. Quality control and assurance

In field, attention was paid to the clothes and gloves worn, which were in cotton. Only the boots were made of plastic. Field equipment was washed with water and hexane/acetone to remove plastic residues or additive contamination. To prevent contamination in laboratory, cotton lab coats and nitrile gloves were worn during handling samples. All the work surfaces and apparatus were cleaned with distilled water

and/or appropriate solvent before usage. Glass containers and beakers were rinsed with distilled water and fluxed with compressed air. The samples were covered with aluminum foil or closed in glass containers during stirring, decantation and filtration steps. During the microscopical observation and FTIR analyses, cotton lab coats and nitrile gloves were worn.

3. Results and discussion

3.1. Characterization of the pristine mulching film

3.1.1. Radiometric properties

Table S3 shows the radiometric coefficients obtained from the laboratory tests. To reduce weed growth, a black MF must be opaque to PAR radiation, i.e., it must have a very low PAR transmissivity coefficient (Malinconico et al., 2008; Vox and Schettini, 2007). BIO-0 showed a very low PAR transmissivity coefficient equal to 0.12 %. MFs characterized by a low LWIR transmissivity coefficient have a high capacity to reduce LWIR losses from the mulched soil (Vox et al., 2005). The lower the LWIR transmissivity coefficient of the MF, the higher the soil temperature under the MF. BIO-0 film showed a rather low LWIR transmissivity coefficient equal to 15.87 %.

3.1.2. Chemical characterization

The samples were characterized by mass spectrometry (MALDI-TOF, Py-GC–MS, and ICP-MS) and thermal analysis (TG and DSC) to determine the polymeric nature and inorganic matter content. In addition, the MMs and their distribution were also assessed to evaluate the extent of chain cleavage during sample irradiation.

To determine the identity of the polymeric part of the MF, the latter was extracted with $CHCl_3$ and analyzed by MALDI-TOF. As shown in **Fig. S2**, the MALDI-TOF spectrum of BIO-0 revealed the presence of the poly(butylene-adipate-*co*-terephtalate) (PBAT) copolyester. The mass peaks belong to sodium adducts of cyclic copolymeric species and oligomers with acid/alcoholic end groups. Their structure, co-monomer ratio (A/T), and mass/charge (m/z) are reported in **Table S4.** It is worth noticing that MALDI-TOF detects preferentially macromolecules at low mass range when applied to polydisperse polymers (Montaudo et al., 2004; Montaudo et al., 2005). Thus, these assignments are related to the PBAT oligomers within the polymeric bulk. Nevertheless, as reported below, relevant information can be achieved by recognizing polymeric structure, especially compared to aged samples.

To gather further information on the material composition, TD and Py-GC–MS analyses were performed at different temperatures, allowing the identification of both additives and polymeric pyrolysis products (Fig. 1a and **Fig. S3**). Table 1 reports the degradation products identified

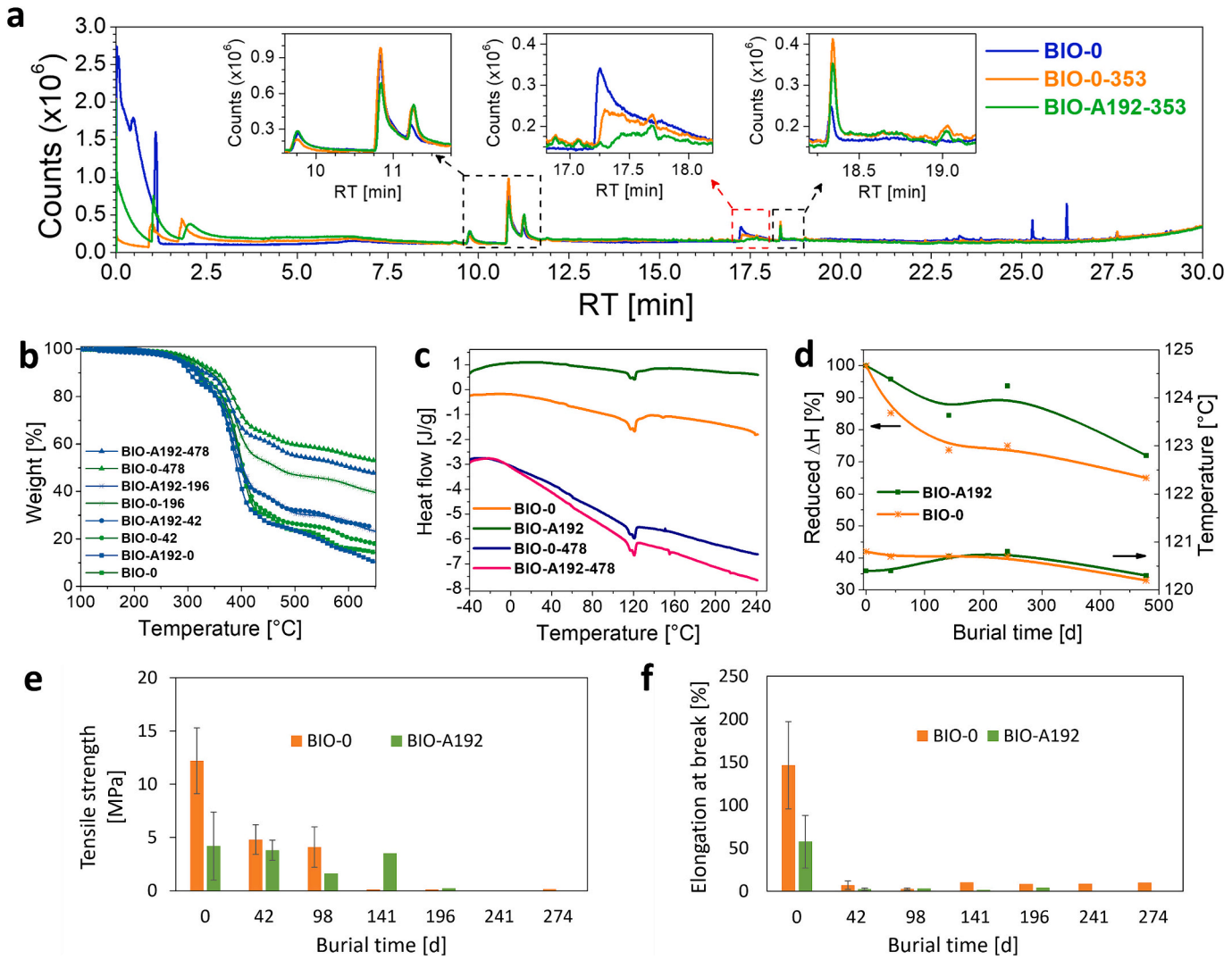

Fig. 1. a) TD-GC–MS of: BIO-0 sample (blue profile), BIO-0-353 (orange profile) and BIO-A192–353 (green profile) collected at 300 °C. b) TG curves of BIO-0 and BIO-A192, neat and after 42, 196 and 478 days of burial. c) DSC thermograms of the second heating scan of BIO-0, BIO-A192, BIO-0-478, and BIO-A192–478. Change in: d) melting enthalpies and temperatures of the PBAT fraction, e) tensile strength (TS), and f) elongation at break (EB), of BIO-0 and BIO-A192 upon soil burial.

Table 1
BIO-0 pyrolysis products identified at 300 °C and 400 °C by TD and Py-GC–MS.

TD-GC–MS Temperature [°C]	Compound	Formula	RT	M_W
300	3,6-Dimethyl-1,4-dioxane-2,5-dione (meso-form) (polymer thermal degradation product_PLA)	$C_6H_8O_4$	9.8	144.13
	3,6-Dimethyl-1,4-dioxane-2,5-dione (DL-form) (polymer thermal degradation product_PLA)	$C_6H_8O_4$	10.8	144.13
	Levoglucosan (degradation compound of starch)	$C_6H_{10}O_5$	17.2	162.14
	1,6-Dioxacyclododecane-7,12-dione (Adipic thermal degradation product)	$C_{10}H_{16}O_4$	18.3	200.23
	1-Propene-1,2,3-tricarboxylic acid, tributyl ester (hydrolysis product of Tributyl acetyl citrate)	$C_{18}H_{30}O_6$	25.3	342.42
	Tributyl acetyl citrate (plasticizer)	$C_{20}H_{34}O_8$	26.2	402.48
400	THF	C_4H_8O	2.0	72.11
	Adipic ketone	C_5H_8O	4.2	84.12
	1,6-Dioxacyclododecane-7,12-dione (polymer thermal degradation product)	$C_{10}H_{16}O_4$	18.3	200.23
	Adipic acid, dicyclobutyl ester (polymer thermal degradation product)	$C_{14}H_{22}O_4$	20.7	254.32
	Monobut-3-enyl phthalate (polymer thermal degradation product)	$C_{12}H_{12}O_4$	21.8	220.22
	Terephthalic acid, di(but-2-enyl) ester	$C_{16}H_{18}O_4$	24.0	274.31
	Terephthalic degradation product (polymer thermal degradation product)		27.2	
	Adipic degradation product (polymer thermal degradation product)		32.3	
	Adipic degradation product		33.3	
	Terephthalic degradation product (polymer thermal degradation product)		37.0	

at 300 °C and 400 °C.

At 300 °C, several peaks deriving from the thermal degradation of PBAT were present (Fig. 1a**)**. Specifically, the peak at retention time (RT) equal to 18 min was assigned to 1,6-dioxacyclododecane-7,12-dione formed by the degradation of the butylene adipate chains (De Falco et al., 2023). The peak at RT 26.2 min was assigned to tributyl acetyl citrate used as a biodegradable plasticizer (Table 1). At 400 °C, the chromatogram showed peaks mostly deriving from the decomposition of the butylene terephthalic chains of PBAT copolymer, further corroborating MALDI-TOF data (**Fig. S3**).

Interestingly, in addition to the presence of PBAT, signals deriving from the degradation of polylactic acid (PLA) at RT of 9.8 and 10.8 min were unambiguously detected (Fig. 1a). The lack of such information in MALDI-TOF often occurs for PLA-based blends (Puglisi et al., 2023), since the MALDI-TOF process suffers from polymer preferential desorption depending on the blend formulation. As it turns out, Py-GC–MS resulted more suitable for the whole qualitative characterization of such polymer blends. Finally, a broad peak ranging from 15 to 16.5 min was assigned to levoglucosan (Table 1). The latter indicated the presence of starch within the material formulation (Zhang et al., 2013; Yu et al., 2019).

The BIO-0 MF was then subjected to acid digestion, and ICP-MS analysis was performed to identify and quantify the metal ions content. As it is noticed from **Table S5**, about 8000 mg/kg of Ca were found, likely due to the presence of $CaCO_3$ used as filler. The sample did not contain relevant content of toxic metal ions, whereas 101 mg/kg of Zn was present. The latter might derive from the phenylphosphonic acid zinc salt, used for manufacturing plastic products due to its ability to improve crystallization, mechanical properties, and biodegradation in various polymers (Wang et al., 2020).

Thermal characterization of BIO-0 was carried out by means of TG and DSC. Fig. 1b presents the TG thermograms, while **Fig. S4** shows the corresponding differential thermograms (DTG). Furthermore, the thermal parameters calculated from the curves are reported in **Table S6**. The TG and DTG curve analysis of BIO-0 revealed four steps of degradation, consistent with the findings reported by other researchers (Villegas et al., 2023; Venkatesan and Rajeswari, 2016). From these data, initial degradation temperature (temperature at 10 % weight loss, $T_{10\%}$), weight loss (WL) and temperature of the maximum decomposition rate of the observed degradation steps (T_{max}), and the percent residue at 650 °C ($Char_{650}$) were calculated (**Table S6)**. The first step occurred between 280 and 340 °C (T_{max1} = 324 °C), with an associated WL of approximately 17 %, and is typically associated to the decomposition of glucose rings in amylose and amylopectin, which are the components of the starch macromolecules. The second step, with a T_{max2} at 400 °C, corresponds to the degradation of the PLA and the PBAT fractions, the latter mainly involving the PBAT aliphatic portion. This step accounted for about 53 % of WL. Two further minor degradation peaks at 470 °C and 570 °C were also noted (about 14 % WL), which probably represent the volatilization of the residues of aromatic *co*-polyester units (Pavon et al., 2020). Finally, a residue of 14 % was noted, which accounted for the presence of PBAT char, as well as carbon black and inorganic fillers in the MF. Considering that the PBAT residue under nitrogen is typically between 6 and 10 % (Xiang et al., 2019; Pavon et al., 2020), the amount of carbon black and inorganics in the pristine MF could be roughly estimated as 6–8 %.

The second heating scan of the DSC thermogram of the MFs is displayed in Fig. 1c, while the relevant thermal parameters calculated are listed in **Table S7**. The first thermal event visible on the heating curve at around −33 °C was the glass transition of PBAT. In addition, a thermal transition at 55 °C was noted, likely due to the glass transition temperature of PLA (Villegas et al., 2023; Aldas et al., 2020a). Finally, two groups of melting peaks were noticed: a major one at about 120 °C, corresponding to the melting of PBAT fraction, and a small one at around 150 °C, where the melting of PLA or thermoplastic starch takes place. The enthalpy of fusion associated with the PBAT fraction was 15.6 J/g. From the literature, the melting enthalpy (ΔH_m) of PBAT is reported to be 21–23 J/g (Xiao et al., 2009; Pavon et al., 2020); therefore, DSC further confirmed that the amount of PBAT in the MF was about 70 %.

3.2. Characterization of artificially aged mulch film

3.2.1. Radiometric properties

The radiometric coefficients obtained from the laboratory tests are shown in **Table S3**. The artificially aged (BIO-A192) black MF showed a very low PAR transmissivity coefficient equal to 0.01 %, which was lower than that of the BIO-0 film (0.12 %). Therefore, artificial aging decreased the transmissivity properties in the PAR range, improving the ability of the film to reduce weed growth. The BIO-A192 film showed a LWIR transmissivity coefficient of 16.55 %, close to the value recorded by the BIO-0 film (15.87 %); artificial aging left the film properties in the LWIR range basically unchanged.

3.2.2. Chemical characterization

The degradation of the photo-aged sample BIO-A192 was first monitored by measuring the change in MM values. The sample was

treated with $CHCl_3$, and the soluble part was subjected to GPC analysis. In **Fig. S5** and **Table S8,** the collected MMs values are reported. Even after 192 h of UV exposure, molecular weight (M_w) of BIO-A192 decreased by only 3 % if compared to the pristine sample BIO-0. This is reasonable because of the presence of stabilizing additives and carbon black that protect the polymer from UV radiation during photoaging. In addition, the presence of PLA confers high photo-durability to the MF polymeric part.

The MALDI-TOF spectrum recorded for the sample BIO-A192 is reported in **Fig. S6**. The peaks assigned (**Table S4**) belong to oligomers with a copolymer ratio A/T similar to the original sample. Furthermore, new peaks at a low intensity denote the initial occurrence of photo-oxidation processes. Photo-oxidation products identified for BIO-A192 are reported in **Table S4** and coloured in violet in the associated spectra (**Fig. S6b**). Despite the complexity due to the utmost heterogeneity of the systems and the formation of isobaric structures, the new peaks can be assigned to species derived from αH-abstraction and Norrish reactions. Specifically, oligomers containing phenoxy acid were recognized as terminal groups (*m/z* 1449.5253 and 1469.4403). In addition, some unassigned peaks (*m/z* at 1454.0854, 1512.1266, and 1528.1050) with even masses were noted, suggesting the presence of nitrogen within the chains. This can be reasonable due to the use of an anti-hydrolytic agent such as carbodiimide that reacts with the carboxylic end group, inserting new functionalities (Qiao et al., 2021; Rizzarelli and Carroccio, 2009; Carroccio et al., 2004).

The accelerated aging in the climatic chamber caused some changes also in the TG and DTG curves of the MFs (Fig. 1b**, Fig. S4, and Table S6**). Indeed, T_{max1} and T_{max2} decreased to 305 °C and 390 °C, respectively, suggesting that photo-oxidation caused the thermal stability of starch and PBAT to be reduced. This also affected the final residue at 650 °C, which decreased to 10 %, compared with 14 % of the pristine sample. No significant differences were noticed from the DSC curve. However, a slight decrease in ΔH_m (14.2 J/g) was observed, likely due to the cleavage and crosslinking of polymer chains, which could hinder their rearrangement and crystallization (Mistretta et al., 2020; Kijchavengkul et al., 2008).

Regarding the effect of accelerated weathering on the mechanical properties of BIO-0, Fig. 1 displays the change in tensile stress (TS) (Fig. 1e) and strain (EB) (Fig. 1f) of the film. It is noticed that photo-oxidation dramatically affected the mechanical performance of the film. EB dropped by about 55 %, whereas the TS decreased by >70 %. This behaviour can be due to the complex composition of the MF. As already reported, the starch fraction is mainly influenced by photo-oxidation, which causes significant chain scission (Bajer et al., 2013; Touchaleaume et al., 2018), resulting in a remarkable impact on the mechanical strength of the film. On the other hand, irradiation can also favor crosslinking of the PBAT fraction, thereby decreasing the material ductility (Mistretta et al., 2020; Kijchavengkul et al., 2008).

3.3. Degradation in soil

3.3.1. Climatic parameters of the experimental site

The degradation process of the buried material is influenced by many parameters, including external air temperature and soil temperature variations, water content, solar radiation, rainfall, and soil microbial community composition and activity.

The mean, minimum, and maximum values of external air temperature from the start of the experiment are reported in **Fig. S7**. The maximum air temperature recorded in the field was achieved at the final phase of the experiment and experienced only by the last collected specimens. The lowest temperature occurred after the fifth sampling and, therefore, affected only the specimens of the last three samplings.

Soil temperature and water content values recorded during the test are reported in **Table S9**. The monthly maximum values of soil temperature ranged from 13.1 °C (recorded during January 2023) to 35.9 °C (recorded during July 2022) and the monthly minimum values of soil temperature ranged from 4.8 °C (recorded during February 2023) to 22.9 °C (recorded during July 2023). The mean, minimum, and maximum values of soil temperature from the burial to each sampling day are reported in **Fig. S8**. Similarly, the maximum soil temperature occurred when all the specimens were still buried, while the minimum soil temperature was experienced only by the specimens collected during the last three samplings. Concerning the soil water content, the highest maximum and mean values (37.2 % and 33.7 %, respectively) were recorded in May 2023. This is due to the high rainfall of the period; in particular, May 2023 was the rainiest month (132.4 mm of rain) during the test. The lowest values of soil water content were recorded during the first months of the test, with July 2022 having the lowest minimum, maximum, and mean values ever.

Fig. S9 shows the rainfall measured during the test. Overall, 790 mm of rain fell during the test period of 16 months, from June 2022 to September 2023. ISTAT (2024) reported an average value of the total annual precipitation in this area of 570 mm from 2006 to 2015 and 535 mm from 1981 to 2010. Considering the quantity of rain between samplings, the driest period was between the first and the second sampling, with a mean of 0.78 mm of rain per day. The rainiest period was between the sixth and the seventh sampling (3.35 mm per day).

The solar radiative energy at the experimental field is shown in **Fig. S10**. The total radiation was 8049.03 MJ m^{-2} in the test period, with a mean of 16.84 MJ m^{-2} per day. The maximum was measured between the burial and the first sampling (26.10 MJ m^{-2} per day), while the minimum was between the fourth and the fifth samplings (6.75 MJ m^{-2} per day).

3.3.2. Characterization of the buried mulching films

3.3.2.1. Structural characterization. The test ended after 478 days, on 28 September 2023. The pristine and artificially aged materials underwent a visible degradation process in the soil, as shown in Fig. 2. The surface area of each sample clearly presented gaps that increased in size over time for both pristine and artificially aged MFs (Fig. 2a). The average surface loss (%) (mean of 3 replicates) increased in both cases as shown in Fig. 2b. For the pristine material, after 42 days of burial, the surface loss was 1.30 % (2.51 cm^2), reaching 56.70 % (116.0 cm^2) on the last sampling. Concerning the artificially aged material, after 42 days of burial, an average surface loss of 4.55 % (9.1 cm^2) was observed, while it reached 65.90 % (132.9 cm^2) at the end of the experiment.

The GPC measurements showed no remarkable differences in MMs values of the copolyesters fraction during degradation (**Table S8**). The residual polyester portion of both pristine and artificially aged films appeared not to be significantly affected upon burial in terms of polymer chain cleavage. However, it is worth noting that more reliable GPC measurements would require an absolute detection method, especially for copolymeric blends.

Considering the relatively fast deterioration of the films after 42 days (Fig. 2), it was hypothesized that the degradation of starch played a key role in this initial phase of the biodegradation process, while PLA and PBAT components degraded slower than the carbohydrate part. TD-GC–MS analysis corroborated this hypothesis. Indeed, the depletion of the signal belonging to levoglucosan was observed after burial, with its quasi-total disappearance from the chromatographic profile of the sample BIO-A192–353 (Fig. 1a). As reported, artificial aging by UV irradiation decreased the degree of crystallinity and M_w of corn, waxy corn, and wheat starches (Bajer et al., 2013; Touchaleaume et al., 2018). Within the same chromatographic profile, an opposite trend for the peak corresponding to PBAT degradation product 1,6-Dioxacyclododecane-7,12-dione (RT = 18.3 min) was recorded. Moving from BIO-0 to BIO-0-353, as the starch signal dropped down, the PBAT signal increased (Fig. 1a). The 3,6-dimethyl-1,4-dioxane-2,5-dione signals deriving from PLA thermal decomposition were not significantly affected and were still present at the end of the trial (RT = 9.8 min). In contrast, the peaks

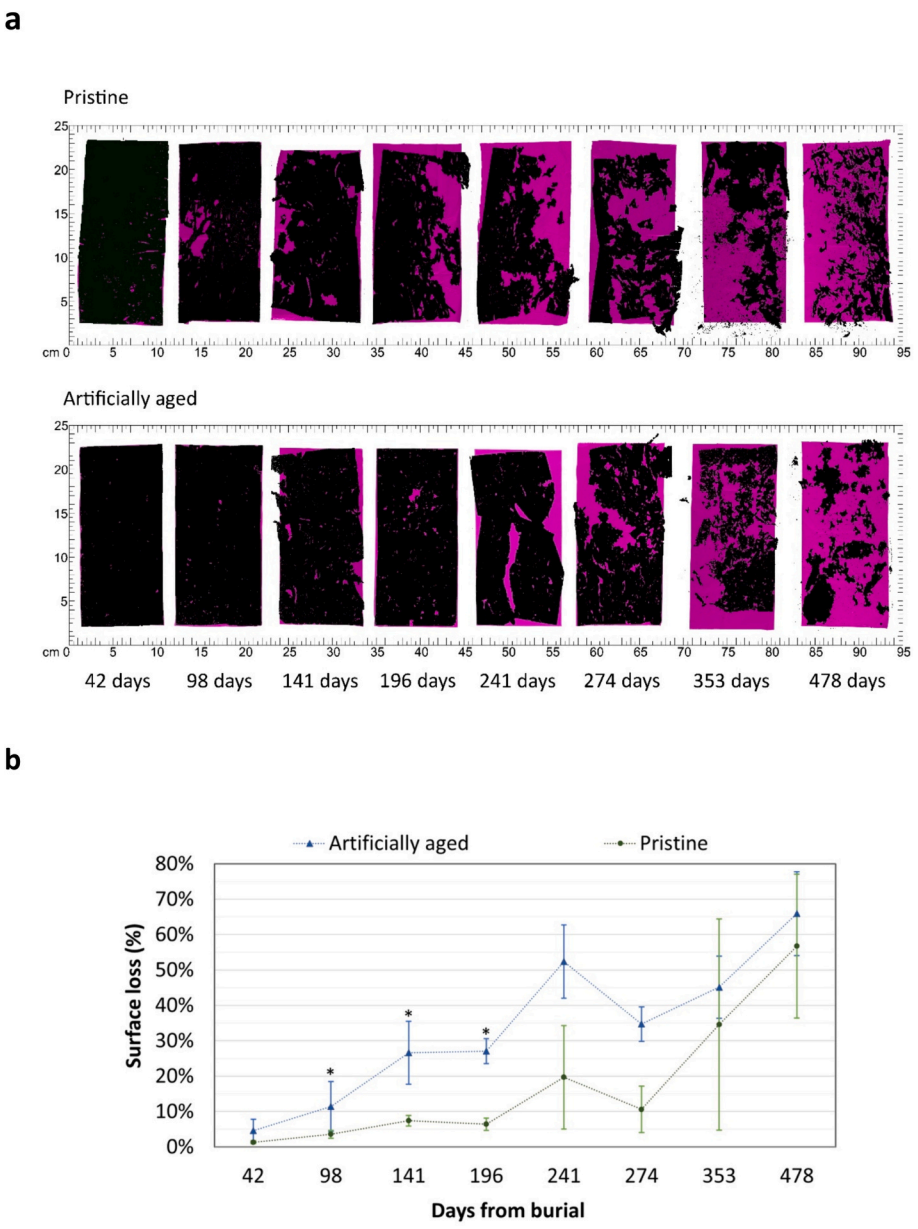

Fig. 2. a) Degradation in the soil of the pristine and artificially aged biodegradable MF specimens: comparison between the same specimen before burial (magenta surface) and after the period in the soil (black surface); b) Surface loss, as percentage difference of areas over burial time, for both the pristine and artificially aged specimens; asterisks indicate significantly different values ($p < 0.05$).

assigned to the plasticizer tributyl acetyl citrate at 25.3 and 26.2 min completely disappeared from the chromatographic profiles of BIO-0-353 and BIO-A192–353. This finding indicated that after 353 days, the organic part of the residual artificially aged film, consisting of fragments ranging from 1.9 to 4.3 mm, is mainly composed by PBAT and PLA.

MALDI-TOF measurements performed on BIO samples provided detailed information at the molecular level on the structural changes in the polymer fraction at the lower MMs range. In **Fig. S11**, the enlargement of MALDI-TOF spectra of BIO-0 **(Fig. S11a)** and BIO-0-353 **(Fig. S11b)** in the *m/z* 1400–1550 mass range is observed. As visible in the spectrum of BIO-0-353, a shift in the adipate-to-terephthalate (A/T) ratio towards higher terephthalic contents is revealed (**Fig. S11b**). Indeed, the peak at *m/z* 1443.6494, belonging to oligomers rich in adipate (6 A/1 T), was clearly detectable in the mass spectrum of the pristine BIO-0 (**Fig. S11a**), while this peak had a very scarce intensity in the spectrum of the specimens that have been buried (**Fig. S11b).** Conversely, in BIO-0 the intensity of the peak at *m/z* 1543.5586 (ratio 1 A/6 T) was weak, becoming more abundant in BIO-0-353.

These data clearly suggest that although not detectable by techniques such as TD, Py-GC–MS, and GPC, the PBAT composition of buried samples was altered at the molecular level at this stage of burial exposure. Specifically, biodegradation of the aliphatic part (butylene adipate units) within the macromolecular chains was promoted, thus enriching the aromatic content of the film residues remaining in the soil. This data was better emphasized by plotting the relative abundance of the peak at *m/z* 1443.6494 (**Fig. S12**). It was also observed that in BIO-A192–353 the selected peak presented a relative abundance higher than the pristine (BIO-0-353). This behaviour might suggest a reduction of the biodegradation rate in photo-exposed samples induced by the formation of new terminal groups less prone to degrade.

3.3.2.2. Thermal properties. Burial did not change significantly T_{max1} of BIO-0 (**Table S6**), however, WL associated to the relative degradation step significantly decreased for BIO-0-196 and BIO-0-478, to 10 and 8 %,

respectively, indicating that >50 % of starch had biodegraded or was released in the soil (Fig. 1b, **Table S6, Fig. S4**). Similarly, WL at the end of the second degradation step (70 %) was almost unchanged after 42 days of burial, then was found to be 47 % and 36 % after 196 and 478 days of burial due to the degradation of the PBAT phase. Finally, the char amount at 650 °C significantly changed, reaching a value of 53 % for the sample buried for the longest time, confirming that about 50 % of the weight of the organic fraction of the MF was removed from the buried sample.

The artificial aging affected the behaviour of the MF during burial. Indeed, the initially rapid WL step associated with starch degradation tended to vanish already after 42 days of burial, and completely disappeared in BIO-A192–478 (**Table S6**), corroborating the evidence from TD-GC–MS about the faster release of starch from the artificially aged film compared to the pristine sample. The WL at day 42 of the experiment was in fact about 60 %, confirming faster degradation in soil with respect to BIO-0. Rather interestingly, this value did not change after 196 days, and even the char value was remarkably lower (24 %) compared to BIO-0 at the same time (40 %), indicating that at longer burial times, the degradation trend of BIO-A192 was slower.

Altogether, this evidence suggests that photo-oxidation could play a dual role. On the one hand, it facilitated the cleavage of the starch chains, accelerating their uptake in the soil. On the other hand, it could cause crosslinking of the macromolecules, particularly the PBAT phase, leading to a retardation of its degradation. Indeed, the char values of the two samples tended to converge only after 478 days. Fig. 1d summarizes the changes in melting enthalpies and temperatures associated with the peak related to the PBAT phase, which was the most abundant, upon the burial of the MF. As shown, for both BIO-0 and BIO-A192, ΔH_m decreased with increasing burial times. In particular, ΔH_m of BIO-0 rapidly decreased by about 25 % after 241 days, due to the degradation of the PBAT phase, and finally by 35 % after 478 days. Considering

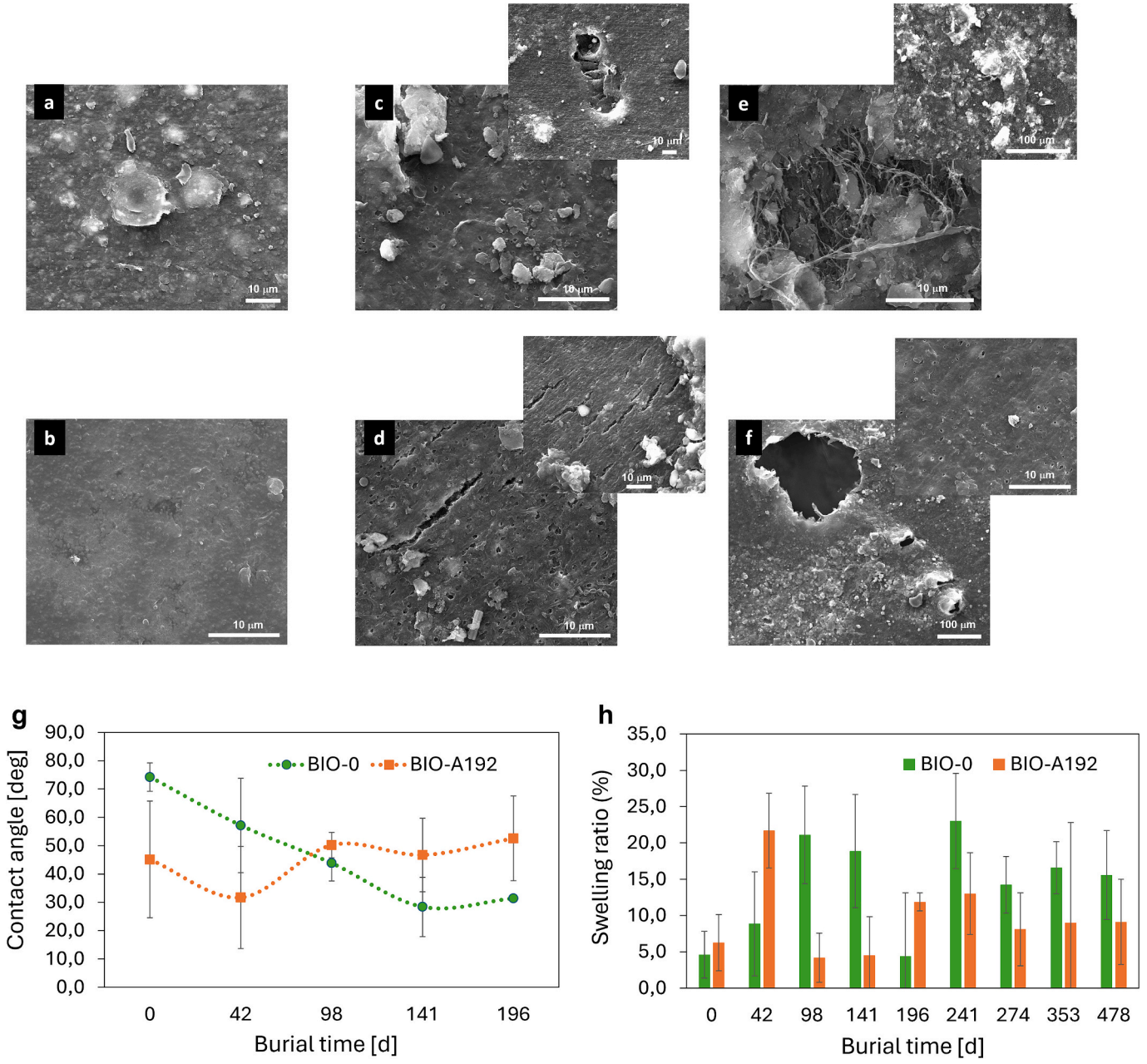

Fig. 3. SEM micrographs of the surface of mulch films: a) BIO-0, b) BIO-A192, c) BIO-0-42, d) BIO-A192–42, e) BIO-0-353, f) BIO-A192–353. Change of: g) water contact angle (WCA), h) swelling ratio of BIO-0 and BIO-A192 upon burial.

that about 6–8 wt% of the MF was represented by inorganics, including binders, $CaCO_3$, and carbon black, and supposing that the ability of PBAT to crystallize did not change upon burial, it can be stated that around 40 % of the initial PBAT was released in the soil. This figure is approximate due to the presence of soil particles firmly attached to the film surface and to the fact that the starch fraction contained in the MF degraded faster than PBAT. The enthalpy changes observed in the case of BIO-A192 were slower (about 10 % after 241 days), since the photo-oxidization process facilitated the release of starch, thereby increasing the relative amount of PBAT in the sample recovered from the soil. However, after a longer time, e.g. 241 days, degradation of PBAT occurred, and the reduced ΔH_m values of the two samples tended to converge. Finally, no significant changes in melting temperature values were observed, even for long burial times, confirming that the PBAT fraction remaining in the MFs maintained its structural integrity, even after 478 days.

3.3.2.3. Scanning Electron Microscopy. Morphological analysis was performed by SEM observation of the film surfaces. Both pristine and artificially aged samples buried for different periods in soil were examined, to evaluate the effect of artificial photo-oxidation and burial on the morphological features of the MF surface (Fig. 3). Both BIO-0 (Fig. 3a) and BIO-A192 (Fig. 3b) showed a homogeneously rough surface, featuring many particles with sizes in a 2–10 mm range evenly distributed throughout the film surface. The latter were likely due to starch granules, carbon black, and inorganic fillers (mainly calcium carbonate) introduced to improve the properties of the blend between PBAT and thermoplastic starch (Lackner et al., 2021). No significant effects were ascribed to the photo-oxidative aging, as before burial BIO-A192 showed a morphology comparable to that of the pristine sample BIO-0. During the field test (upon burial), formation of cracks and tearing of the film surfaces were observed, indicating the progressive loss of integrity of the material. Already after 42 days of burial, both pristine and photo-oxidized samples exhibited the formation of large cracks and voids due to the removal of particles from the surface. The comparison of BIO-0-42 **(**Fig. 3c**)** and BIO-A192–42 **(**Fig. 3d**)** highlighted the pro-degradative effect of artificial aging, as the latter showed a higher number of cavities and larger cracks. As already reported by several authors (Malinconico et al., 2008) who studied the field-aging of starch-based MFs, the disappearance of starch granules is the first step in the degradation process of polyester-starch blends. These starch granules were initially regularly distributed within the synthetic polymeric matrix, and their release and consumption by hydrolytic processes and soil microorganisms resulted in the formation of defects at the surface of the PBAT/starch film. As a matter of fact, the biodegradation process is favoured by swelling due to water absorption of the hydrophilic starch fraction. This surface deterioration is considered the first step of the biodegradation mechanism, which modifies the mechanical, physical, and chemical properties of the material (Lucas et al., 2008).

It was noticed that the polymer matrix surrounding these granules degraded slower, however the formation of cracks confirmed that the PBAT component was also involved in the film degradation. At longer burial times (**Fig. S13**), the film surface exhibited massive colonization by soil microorganisms, which could further accelerate polymer biodegradation by metabolic or enzymatic action (Agustin-Salazar et al., 2022). Indeed, BIO-0-353 **(**Fig. 3e**)** showed a massively eroded polymer surface since, underneath the soil residues and the biofilm developed upon burial, the visible cracks were larger and more numerous, accounting for the progressive removal of a significant fraction of the former surface. Similar features were also observed for BIO-A192–353, where degradation even caused the formation of macroscopic holes (Fig. 3f). However, rather surprisingly, several regions of this sample exhibited a more homogeneous surface, with a lower number of remarkable erosion features and an appearance comparable to that of the samples retrieved from the soil after shorter time periods. This apparently odd outcome can be related to the impact of accelerated weathering, which induces both main chain scission of starch and PBAT, as well as crosslinking of the PBAT fraction (Kijchavengkul et al., 2010a). In particular, as demonstrated by GC–MS analysis, photo-oxidation of BIO-0 induced massive chain scission of starch, causing its faster removal from the MF upon burial (La Mantia et al., 2020). Since starch facilitates film degradation by favouring humidity absorption, microorganism attachment, and micro-cracking, this entails that at longer burial times, the composition of the BIO-A192 films was progressively enriched in a partially crosslinked PBAT fraction, richer in aromatic moieties, which degraded slower and was less prone to the microbial attachment.

3.3.2.4. Water Contact Angle and swelling ratio. WCA measurements were performed on buried samples at different times to assess the possible changes in hydrophilicity of the surface of BIO-0 and BIO-A192 films. The tests were carried out up to 196 days of burial (Fig. 3g), since the surface of the samples retrieved at longer times was heavily degraded, to the point that those specimens immediately absorbed the water drop preventing the measurement. From Fig. 3g, it is noted that for BIO-0, the WCA value constantly decreased with the soil burial time, from an initial 78° to 32° after 196 days. That is, soil burial favoured the wettability of the films, due to the hydrolysis of the substrate with the consequent formation of polar functional groups (La Mantia et al., 2020; Aldas et al., 2020b). Photodegradation during artificial aging induced a dramatic decrease of WCA (45° for BIO-A192), which is related to the chain scission-induced formation of carbonyl and hydroxyl groups. Interestingly, in the latter case the WCA values did not vary significantly with increasing burial times. Indeed, the relative increase of PBAT content in the film due to the faster mineralization of the polar starch fraction counterbalanced the rise in wettability observed in the buried BIO-0 samples.

A more detailed insight into the degradative behaviour of buried BIO-0 and BIO-A192 films was provided by the evaluation of their swelling in water. Generally, water resistance determines the swelling property of materials. It is closely related to the interactions (i.e., hydrogen bonding, covalent bonding, and ionic bonding) between the molecule chains and water (Chen et al., 2021). Upon burial, a trend to increased water absorption is generally expected, however in a complex matrix such as a MF, swelling ratio variations reflect the occurrence of specific changes in the film structure. In Fig. 3h, the average values of the swelling ratio of the two samples are reported as a function of the burial time. As regards BIO-0, a value of about 5 % weight gain was recorded before burial (Mostafa and Sourell, 2009). Upon burial, hydrolytic reactions took place, resulting in the formation of hydroxyl and carboxyl groups, which favoured water absorption, and attained a value of 21 % after 98 days. At the same time, starch chains, which were cleaved faster than PBAT, were progressively released from the matrix, causing the swelling ratio to drop until a minimum of 4.4 % attained after 196 days. From here onward, the combined hydrolytic/biotic degradation of the PBAT phase proceeded, associated with a significant increase of water absorption due to the formation of hydrophilic oligomer species (16.5 % after 353 days). In comparison, BIO-A192 showed faster variations in swelling ratios. Before burial, a value of 6.3 % was recorded due to the photo-oxidative chain scission. This pretreatment strongly favoured moisture absorption of the buried film, which showed a maximum value of about 22 % after 42 days of burial. The high-water uptake further accelerated the release of the degraded starch chains, so that the film reached the minimum swelling ratio of 4.4 % already after 98 days (compared with 196 days of pristine BIO-0). Subsequently, degradation of PBAT took place, and swelling values increased, yet to a lower extent compared to BIO-0, owing to the lower content of starch remaining in the MF.

3.3.2.5. Mechanical characterization: tensile tests. EB and TS of BIO-

0 and BIO-A192 films periodically removed from the experimental field up to 274 days of burial are reported in Fig. 1e, f. It was not possible to perform tensile tests for the samples buried for longer times as these specimens were too brittle and failed after recovery from the soil. Both samples displayed a dramatic decrease in ductility upon burial. For BIO-0, EB decreased from 150 % to 7 % after 42 days, and it remained rather constant, around 10 % until 274 days of burial. Lower values were measured for BIO-A192, with EB averaging 2.5 % between day 42 and day 274. Moreover, the samples failed prematurely compared to BIO-0, and mechanical characterization could be carried out until 196 days of burial. Interestingly, buried BIO-A192 retained the original value of TS for a longer time than BIO-0. This evidence can be related to the crosslinking of PBAT triggered by the UV irradiation which allowed BIO-A192 to keep its mechanical properties to a certain extent even after prolonged burial.

3.3.3. *Microplastics isolation and identification in the soil*

Besides the characterization of the macroscopic film residues remaining in the soil after burial, the microplastics fraction contained in the soil was also characterized, to get information on the possible changes occurred in structure and composition of the material released in the soil upon burial. To isolate microplastics from soils, the oil-based separation approach applied by Crichton et al. (2017) was used. With this approach, microplastics are extracted in the oil phase due to their lipophilic properties. In general, the oleo-extraction has been proven to be efficient, replicable, and accurate for several environmental matrices (Corami et al., 2021; Rosso et al., 2023). In particular, microplastic separation using canola oil has been reported to be an optimal method to recover microplastics of different compositions (Radford et al., 2021). The canola oil separation approach, the double filtration procedure, the digestion of organic matter with hydrogen peroxide adopted in this work were not an easy procedure and, in some case, these steps were not optimal to identify the chemical composition of the recovered fragments due to oil residue and to nitrocellulose contamination (due to the first filtration step) hindering FTIR analysis. Notwithstanding these drawbacks, the applied protocol allowed for the recovery of black fragments from the soil, in which MF was buried, on silicon filter (Fig. 4a, d), and enabled to identify their chemical composition, attributed to the buried films with a high level of confidence, using FTIR microspectroscopy. No interference with soil organic matter was observed, which could have hindered their chemical identification using FTIR spectroscopy. FTIR spectra were acquired on an area of 50 μm × 50 μm, which allowed to analyze the microplastics present, having size ranging from 80 to 1500 μm, and to obtain spectra with an optimal signal/ratio. The analysis of the isolated fragments (Fig. 4b, e) indeed presented the main absorption bands of the starting polymer. The main functional groups of the biodegradable polymers were easily identified and verified also by matching the spectrum with FTIR spectral database by using Thermo Scientific OMNIC™ Spectra™ software. In details, the FTIR spectra of fragments isolated from the soil in which BIO-0 was buried (Fig. 4c), coded as SOIL-BIO-0, were characterized by absorption bands centered at 2920 cm^{-1} and 2850 cm^{-1}, due to the asymmetric and symmetric stretching vibration of CH_2 groups, respectively, at 1714 cm^{-1}, assigned to the stretching vibration of C=O group, at 1504 cm^{-1} and 1459 cm^{-1} due to the characteristic stretching of the C=C phenylene group, at 1410 cm^{-1} and 1391 cm^{-1} due to CH_2 bending vibration. Absorptions at 1279 cm^{-1} and 1169 cm^{-1} were assigned to the symmetric stretching vibration of C–O, at 1122 cm^{-1} and 1106 cm^{-1} to C–O left-right symmetric stretching vibration absorption, and at 1019 cm^{-1} to in-plane bending vibration, at 872 cm^{-1} and 728 cm^{-1} to out-of-plane bending vibration of the phenylene ring (Tavares et al., 2018). The same absorption bands were identified in the FTIR spectra of fragments isolated from the soil in which BIO-A192 was buried, coded as SOIL-BIO-A192 (Fig. 4f). No fragments were isolated by applying the oil-based separation approach on the control sample, SOIL-0, soil sampled in an area without buried specimens.

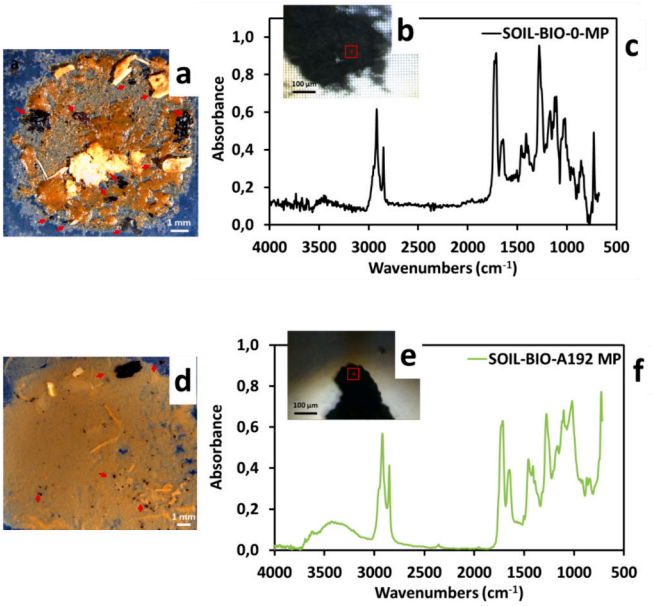

Fig. 4. Isolation and identification of microplastics(MPs): a) optical micrograph of silicon filter containing fragments isolated from SOIL-BIO-0; b) optical micrograph of an isolated fragment on which the red square indicates the FTIR acquisition area; c) FTIR spectrum of fragment isolated from SOIL-BIO-0; d) optical micrograph of silicon filter containing fragments isolated from SOIL-BIO-A192; e) optical micrograph of an isolated fragment on which the red square indicates the FTIR acquisition area; f) FTIR spectrum of fragment isolated from SOIL-BIO-A192.

Given the above mentioned drawbacks of the adopted oil-based separation approach, the quantification of the MF degradation products released to soil during MF burial was performed by dispersing a larger amount of soil in $CHCl_3$, and analyzing the solution containing the MF degradation products by means of TG.

The quantitative TG analysis of MF degradation products extracted in $CHCl_3$ from the soil in which the MFs were buried, coded as sSOIL-BIO-0 and sSOIL-BIO-A192 (Fig. 5a, b), showed a thermal degradation behaviour comparable to those obtained from neat polymers dissolved in $CHCl_3$, sBIO-0 and sBIO-A192. A strong shift to lower temperature of the degradation steps was however observed in the thermograms of materials extracted from SOIL-BIO-0 and SOIL-BIO-A192, probably due to the occurrence of degradation of the polymeric phase in the soil samples. The amount of the extracted phase from soils was determined by the WL occurring in the range 70–650 °C. The results indicate that it was possible to extract 3.9 ± 1.2 μg/μL and 3.0 ± 0.2 μg/μL of polymeric fractions from SOIL-BIO-0 and SOIL-BIO-A192, respectively. Reporting these concentrations to the amount of soil samples it is possible to assess that, depending on the MF used, the contamination could range from 79 ± 25 to 60 ± 4 mg of BIO-0 and BIO-A192 residues, respectively, per kg of soil (i.e. 0.008 % and 0.006 % mass-based). However, these figures should be considered as approximate due to the possible presence of soil extractives and to the limited solubility of the crosslinked PBAT fraction.

FTIR spectra of sSOIL-BIO-0 and sSOIL-BIO-A192 (Fig. 5c, d) allowed to identify that the components extracted from soil samples mainly consisted of the aliphatic moieties of PBAT. With respect to sBIO-0 and sBIO-A192 spectra, sSOIL–BIO-0 and sSOIL-BIO-A192 spectra were indeed characterized by an increase in the absorbance of the bands at 2920 and 2850 cm^{-1} due to stretching vibration of CH_2 groups due to the aliphatic chains or other soil extractives, and a shift to higher wavenumber of the absorption band due to carbonyl stretching. The shift of the carbonyl band at 1730 cm^{-1} could be ascribed to the formation of free C=O, while the presence of a shoulder at 1717 cm^{-1} could be ascribed to the formation of lower molecular weight esters

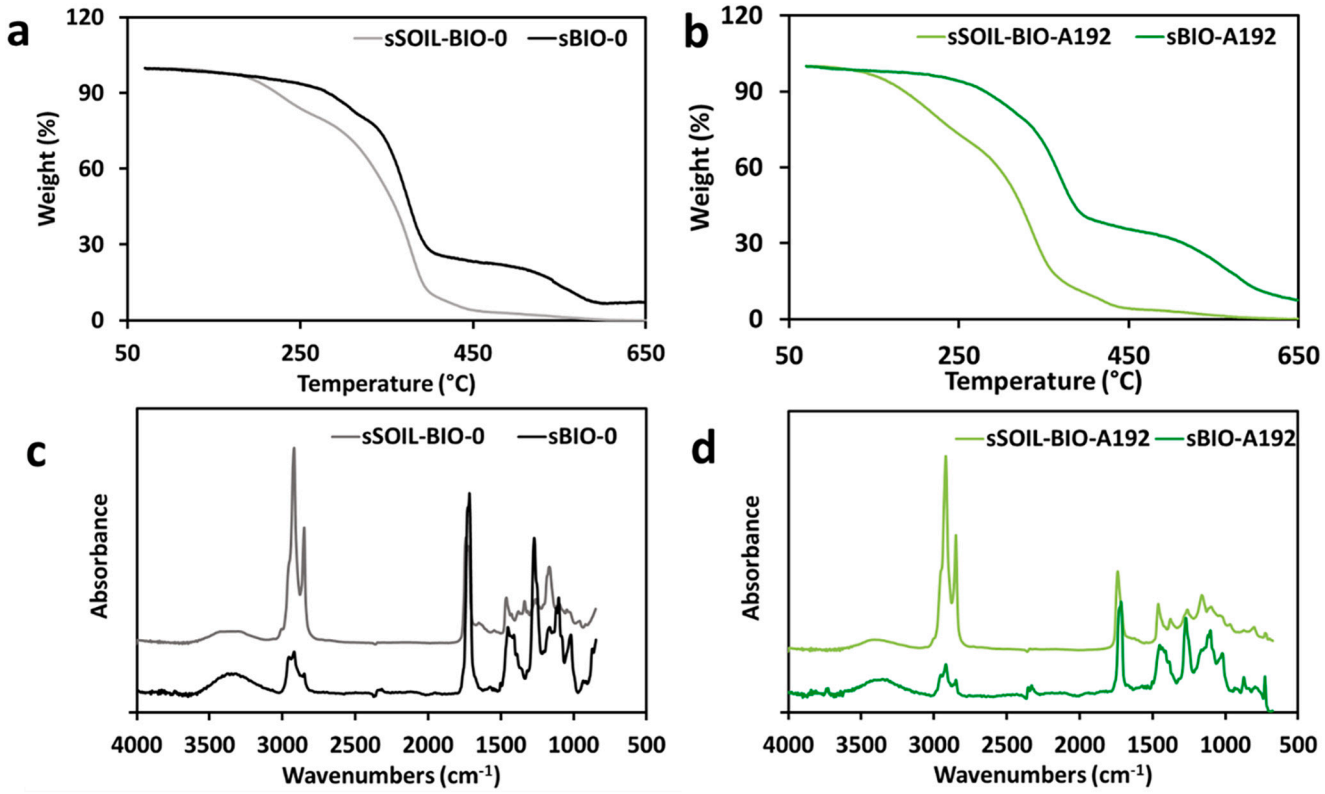

Fig. 5. TG curves of: a) BIO-0 solubilised in $CHCl_3$, sBIO-0, and components extracted from SOIL-BIO-0, sSOIL-BIO-0; b) BIO-A192 solubilised in $CHCl_3$, sBIO-A192 and components extracted from SOIL-BIO-A192, sSOIL-BIO-A192; c) FTIR spectra of sBIO-0 and sSOIL-BIO-0; d) FTIR spectra of sBIO-A192 and sSOIL-BIO-A192.

(Kijchavengkul et al., 2010b). This data confirms the occurrence of Norrish I chain scission during PBAT degradation as also indicated by MALDI-TOF analysis. The absorption bands related to the terephthalic moieties due to the vibration of the phenylene ring were not visible in the sSOIL-BIO-0 and sSOIL-BIO-A192 spectra.

Therefore, in agreement with MALDI-TOF results, FTIR spectra of the extracted components indicated that soil samples were mainly contaminated by MF degradation products rich in adipate while the aromatic part of the copolymers was less abundant, and thus less visible, in the FTIR spectra.

These results confirm that during burial the biodegradation of the aliphatic counterpart (butylene adipate units) occurs in the MFs causing the enrichment of underlying soil with oligomeric/polymeric aliphatic phase. Moreover, the higher concentration of polymeric contamination identified in SOIL-BIO-0 suggests a higher degradation rate of BIO-0 than BIO-A192.

4. Conclusions

In conclusion, the investigation into the degradation of biodegradable MFs under burial conditions provided valuable insights into the complex interplay of environmental factors influencing the fate of these materials. The environmental parameters, such as air and soil temperatures, water content, solar radiation, and rainfall, were meticulously recorded, as they impact significantly on the degradation of the buried materials. Structural characterization of the buried MFs revealed a progressive deterioration, with surface loss and changes in mechanical properties over time. However, film degradation was not complete, and macroscopic residues were still present in the soil even after 16 months of burial. Interestingly, GPC measurements indicated no significant changes in the polyester fraction of the film remaining in the soil, however, TD-GC–MS, MALDI-TOF, and thermal property analysis unveiled molecular alterations at the polymer level, particularly in the aliphatic counterpart, indicating that the film fragments remaining in the soil were progressively enriched in aromatic moieties. Artificial UV irradiation prior to burial induced changes, particularly in starch biodegradation, impacting the composition of the film residues. In particular, accelerated aging could enhance cleavage of the starch chains, facilitating their uptake in the soil. On the other hand, it could cause crosslinking of the polyester phase of the MF, retarding the degradation of PBAT.

One of the first attempts to isolate and characterize microscopic residues of the films released to soil is presented here. Despite challenges in isolation protocols, FTIR and thermogravimetric analysis revealed the presence of MF degradation products, predominantly rich in adipate, further confirming the differential degradation rate between the MFs.

This study provides a comprehensive investigation into the fate of biodegradable MFs in agricultural soil. The results highlight the complex nature of these films, with diverse components influencing their behaviour during degradation. The accelerated aging process mimics real-world conditions, shedding light on the potential environmental impact of biodegradable MFs. Further research is needed to assess long-term impacts on soil health, food security, and ecosystem multifunctionality, considering the diverse factors influencing degradation in real soil conditions.

CRediT authorship contribution statement

Fabiana Convertino: Writing – review & editing, Writing – original draft, Validation, Methodology, Formal analysis, Data curation, Conceptualization. **Sabrina Carola Carroccio:** Writing – review & editing, Writing – original draft, Supervision, Methodology, Funding acquisition, Data curation, Conceptualization. **Maria Cristina Cocca:** Writing – review & editing, Writing – original draft, Validation, Methodology, Formal analysis, Data curation, Conceptualization. **Sandro Dattilo:** Methodology, Formal analysis, Data curation. **Anna Chiara**

Dell'Acqua: Validation, Data curation. **Luca Gargiulo:** Validation, Formal analysis, Data curation. **Luca Nizzetto:** Writing – review & editing, Funding acquisition. **Paolo Maria Riccobene:** Formal analysis. **Evelia Schettini:** Writing – review & editing, Writing – original draft, Supervision, Methodology, Funding acquisition, Conceptualization. **Giuliano Vox:** Writing – review & editing, Writing – original draft, Supervision, Methodology, Conceptualization. **Domenico Zannini:** Validation, Formal analysis, Data curation. **Pierfrancesco Cerruti:** Writing – review & editing, Writing – original draft, Validation, Supervision, Methodology, Funding acquisition, Data curation, Conceptualization.

Declaration of competing interest

The authors declare that they have no known competing financial interests or personal relationships that could have appeared to influence the work reported in this paper.

Data availability

The data that has been used is confidential.

Acknowledgments

This study has received funding from the PAPILLONS project funded under European Union's Horizon 2020 RESEARCH and Innovation Programme (Grant Agreement No 101000210).

The authors thank D. Sfregola, technician of the University of Bari, for his cooperation in the spectrophotometric measurements.

Appendix A. Supplementary data

Supplementary data to this article can be found online at https://doi.org/10.1016/j.scitotenv.2024.174697.

References

Agustin-Salazar, S., Ricciulli, M., Ambrogi, V., Cerruti, P., Scarinzi, G., 2022. Thermomechanical properties and biodegradation behavior of Itaconic anhydride-grafted PLA/pecan nutshell biocomposites. Polymers 14, 5532. https://doi.org/10.3390/polym14245532.

Aldas, M., Ferri, J.M., Lopez-Martinez, J., Samper, M.D., Arrieta, M.P., 2020a. Effect of pine resin derivatives on the structural, thermal, and mechanical properties of mater-bi type bioplastic. J. Appl. Polym. Sci. 137, 48236 https://doi.org/10.1002/app.48236.

Aldas, M., Rayón, E., López-Martínez, J., Arrieta, M.P., 2020b. A deeper microscopic study of the interaction between gum rosin derivatives and a mater-bi type bioplastic. Polymers 12, 226. https://doi.org/10.3390/polym12010226.

ARIF, 2024. Regional Agency for Irrigation and Forestry Activities website. https://www.agrometeopuglia.it/.

Bajer, Dagmara, Kaczmarek, Halina, Bajer, Krzysztof, 2013. The structure and properties of different types of starch exposed to UV radiation: a comparative study. Carbohydr. Polym. 98 (1), 477–482. https://doi.org/10.1016/j.carbpol.2013.05.090.

Carroccio, Sabrina, Rizzarelli, Paola, Puglisi, Concetto, Montaudo, Giorgio, 2004. MALDI investigation of Photooxidation in aliphatic polyesters: poly(butylene succinate). Macromolecules 37 (17), 6576–6586. https://doi.org/10.1021/ma049633e.

Chen, Liang & Qiang, Taotao & Chen, Xuejun & Ren, Wenqi & Zhang, Hui. (2021). Fabrication and evaluation of biodegradable multi-cross-linked mulch film based on waste gelatin. Chem. Eng. J. 419. paper n 129639. doi:https://doi.org/10.1016/j.cej.2021.129639.

Chinaglia S., Esposito E., Tosin M., Pecchiari M., Degli Innocenti F. Biodegradation of plastics in soil: the effect of water content. Polym. Degrad. Stab., 2024, paper n 110691, doi:https://doi.org/10.1016/j.polymdegradstab.2024.110691.

Corami, F., Rosso, B., Morabito, E., Rensi, V., Gambaro, A., Barbante, C., 2021. Small microplastics (< 100 μm), plasticizers and additives in seawater and sediments: oleo-extraction, purification, quantification, and polymer characterization using Micro-FTIR. Sci. Total Environ. 797, 148937 https://doi.org/10.1016/j.scitotenv.2021.148937.

Crichton, Ellika, Noel, Marie, Gies, Esther, Ross, Peter, 2017. A novel, density-independent and FTIR-compatible approach for the rapid extraction of microplastics from aquatic sediments. Anal. Methods 9. https://doi.org/10.1039/C6AY02733D.

De Falco Francesca, Nacci Tommaso, Durndell Lee, Thompson, Richard C., Degano Ilaria, Modugno Francesca. A thermoanalytical insight into the composition of biodegradable polymers and commercial products by EGA-MS and Py-GC-MS, J. Anal. Appl. Pyrolysis, Volume 171, 2023, paper n 105937, doi:https://doi.org/10.1016/j.jaap.2023.105937.

Degli-Innocenti Francesco, Barbale Marco, Chinaglia Selene, Esposito Ermes, Pecchiari Marco, Razza Francesco, Tosin Francesco, Analysis of the microplastic emission potential of a starch-based biodegradable plastic material, Polym. Degrad. Stab., Volume 199, 2022, paper n 109934, doi:https://doi.org/10.1016/j.polymdegradstab.2022.109934.

Escobedo, J.F., Gomes, E.N., Oliveira, A.P., Soares, J., 2009. Modeling hourly and daily fractions of UV, PAR and NIR to global solar radiation under various sky conditions at Botucatu, Brazil. Appl. Energy 86, 299–309. https://doi.org/10.1016/j.apenergy.2008.04.013.

Fan Weixin, Qiu Chunsheng, Qu Qian, Hu Xiangang, Mu Li, Gao Ziwei, Tang XinFan Weixin, Qiu Chunsheng, Qu Qian, Hu Xiangang, Mu Li, Gao Ziwei, Tang Xin, Sources and identification of microplastics in soils, Soil Environ. Health, Volume 1, Issue 2, 2023, paper n 100019, doi:https://doi.org/10.1016/j.seh.2023.100019.

Griffin-LaHue D., Ghimire S., Yu Y., Scheenstra E. J., Miles C. A., Flury M., In-field degradation of soil-biodegradable plastic mulch films in a Mediterranean climate, Sci. Total Environ., Volume 806, Part 1, 2022, paper n 150238, doi:https://doi.org/10.1016/j.scitotenv.2021.150238.

Huang F., Zhang Q., Wang L., Zhang C., Zhang Y. 2023. Are biodegradable mulch films a sustainable solution to microplastic mulch film pollution? A biogeochemical perspective. J. Hazard. Mater., 459, paper n 132024, doi:https://doi.org/10.1016/j.jhazmat.2023.132024.

ISTAT, 2024. *Statistics Italy Ambiente e Energia*. https://www.istat.it/tavole-di-dati/temperatura-e-precipitazione-nei-comuni-capoluogo-di-provincia-anno-2021-serie-storica-2006-2021-normale-climatologica-1981-2010/.

Kijchavengkul, Thitisilp, Auras, Rafael, Rubino, Maria, 2008. Measuring gel content of aromatic polyesters using FTIR spectrophotometry and DSC. Polym. Test. 27, 55–60. https://doi.org/10.1016/j.polymertesting.2007.08.007.

Kijchavengkul, Thitisilp, Auras, Rafael, Rubino, Maria, Selke, Susan, Ngouajio, Mathieu, Fernandez, Rodney, 2010a. Biodegradation and hydrolysis rate of aliphatic aromatic polyester. Polym. Degrad. Stab. 95, 2641–2647. https://doi.org/10.1016/j.polymdegradstab. 2010.07.018.

Kijchavengkul, Thitisilp, Auras, Rafael, Rubino, Maria, Alvarado, Edgar, Camacho Montero, José Roberto, Rosales, Jorge Mario, 2010b. Atmospheric and soil degradation of aliphatic–aromatic polyester films. Polym. Degrad. Stab. 95 (2), 99–107. https://doi.org/10.1016/j.polymdegradstab. 2009.11.048.

Kim Seung-Kyu, Kim Ji-Su, Lee Hwang, Lee Hee-Jee, Abundance and characteristics of microplastics in soils with different agricultural practices: Importance of sources with internal origin and environmental fate, J. Hazard. Mater., Volume 403, 2021, paper n 123997, doi:https://doi.org/10.1016/j.jhazmat.2020.123997.

Kottek, M., Grieser, J., Beck, C., Rudolf, B., Rubel, F., 2006. World map of the Köppen-Geiger climate classification updated. Meteorol. Zeitschrift. 15, 259–263. https://doi.org/10.1127/0941-2948/2006/0130.

La Mantia, F.P., Ascione, L., Mistretta, M.C., Rapisarda, M., Rizzarelli, P., 2020. Comparative investigation on the soil burial degradation behaviour of polymer films for agriculture before and after photo-oxidation. Polymers 12, 753. https://doi.org/10.3390/polym12040753.

Lackner, Maximilian, Ivanič, František, Kováčová, Mária, Chodák, Ivan, 2021. Mechanical properties and structure of mixtures of poly(butylene-adipate-co-terephthalate) (PBAT) with thermoplastic starch (TPS). Int. J. Biobased Plast. 3 (1), 126–138. https://doi.org/10.1080/24759651.2021.1882774.

Li Kang, Jia Weiqian, Xu Libo, Zhang Mengjun, Huang Yi, The plastisphere of biodegradable and conventional microplastics from residues exhibit distinct microbial structure, network and function in plastic-mulching farmland, J. Hazard. Mater., Volume 442, 2023, paper n 130011, doi:https://doi.org/10.1016/j.jhazmat.2022.130011.

Liu, Y., Rillig, M.C., Liu, Q., et al., 2023. Factors affecting the distribution of microplastics in soils of China. Front. Environ. Sci. Eng. 17, 110. https://doi.org/10.1007/s11783-023-1710-4.

Lucas, Nathalie, Bienaime, Christophe, Belloy, Christian, Queneudec, Michèle, Silvestre, Françoise, Nava-Saucedo, José-Edmundo, 2008. Polymer biodegradation: mechanisms and estimation techniques – a review. Chemosphere 73 (4), 429–442. https://doi.org/10.1016/j.chemosphere.2008.06.064.

Malinconico, M., Immirzi, B., Santagata, G., Schettini, E., Vox, G., Scarascia, Mugnozza G., 2008. Chapter 3: An overview on innovative biodegradable materials for agricultural applications. In: Moeller, H.W. (Ed.), Progress in Polymer Degradation and Stability Research. Nova Science Publishers, Inc., NY USA, ISBN 978-1-60021-828-6, pp. 69–114.

Mistretta, M.C., La Mantia, F.P., Titone, V., Botta, L., Pedeferri, M., Morreale, M., 2020. Effect of ultraviolet and moisture action on biodegradable polymers and their blend. J. Appl. Biomater. Funct. Mater. 18 https://doi.org/10.1177/2280800020926653.

Montaudo, G., Carroccio, S., Montaudo, M.S., Puglisi, C., Samperi, F., 2004. Recent advances in MALDI mass spectrometry of polymers. Macromol. Symp. 218, 101–112. https://doi.org/10.1002/masy.200451411.

Montaudo, G., Samperi, F., Montaudo, M.S., Carroccio, S., Puglisi, C., 2005. Current trends in matrix-assisted laser desorption/ionization of polymeric materials. Eur. J. Mass Spectrom. 11 (1), 1–14. https://doi.org/10.1255/ejms.718.

Mostafa, Harby M., Sourell, Heinz, May, 2009. Equilibrium Moisture Content of Some Bioplastic Materials for Agricultural Use (Drip Tubes). In: Agricultural Engineering International: the CIGR Ejournal. Manuscript LW 1180, Vol. XI.

Ng, Ee-Ling, Lwanga, Esperanza Huerta, Eldridge, Simon M., Johnston, Priscilla, Hu, Hang-Wei, Geissen, Violette, Chen, Deli, 2018. An overview of microplastic and nanoplastic pollution in agroecosystems. Sci. Total Environ. 627, 1377–1388. https://doi.org/10.1016/j.scitotenv.2018.01.341.

Pavon, C., Aldas, M., Rosa-Ramírez, H.D.L., López-Martínez, J., Arrieta, M.P., 2020. Improvement of PBAT processability and mechanical performance by blending with pine resin derivatives for injection moulding rigid packaging with enhanced hydrophobicity. Polymers 12 (12), 2891.

Puglisi, R., Scamporrino, A.A., Dintcheva, N.T., Filippone, G., Bruno, E., Scarfato, P., Cerruti, P., Carroccio, S.C., 2023. Photo- and water-degradation phenomena of ZnO bio-blend based on poly(lactic acid) and polyamide 11. Polymers 15, 1434. https://doi.org/10.3390/polym15061434.

Ruimin Qi, Yuanyuan Tang, Jones Davey L., Wenqing He, Changrong Yan, Occurrence and characteristics of microplastics in soils from greenhouse and open-field cultivation using plastic mulch film, Sci. Total Environ., Volume 905, 2023, paper n 166935,doi:https://doi.org/10.1016/j.scitotenv.2023.166935.

Liyuan Qiang, Huibing Hu, Guoqiang Li, Jianlong Xu, Jinping Cheng, Jiaping Wang, Ruoyu Zhang, Plastic mulching, and occurrence, incorporation, degradation, and impacts of polyethylene microplastics in agroecosystems. 2023. Ecotoxicol. Environ. Saf. 263, paper n 115274 doi:https://doi.org/10.1016/j.ecoenv.2023.115274.

Qiao, Runmeng, Wang, Xin, Qin, Guangjiong, Liu, Jialei, Cao, Aocheng, Canbin, Ouyang, He, Wenqing, 2021. Degradation mode of PBAT mulching film and control methods during its degradation induction period. Mini-Rev. Org. Chem. 18 https://doi.org/10.2174/1570193X18666210813142022.

Radford, F., Zapata-Restrepo, L.M., Horton, A.A., Hudson, M.D., Shaw, P.J., Williams, I. D., 2021. Developing a systematic method for extraction of microplastics in soils. Anal. Methods 13 (14), 1695–1705.

Rizzarelli, Paola, Carroccio, Sabrina, 2009. Thermo-oxidative processes in biodegradable poly(butylene succinate). Polym. Degrad. Stab. 94 (10), 1825–1838. https://doi.org/10.1016/j.polymdegradstab, 2009.06.007.

Rosso, B., Corami, F., Barbante, C., Gambaro, A., 2023. Quantification and identification of airborne small microplastics (<100 μm) and other microlitter components in atmospheric aerosol via a novel elutriation and oleo-extraction method. Environ. Pollut. 318, 120889 https://doi.org/10.1016/j.envpol.2022.120889.

Schettini, E., Vox, G., 2012. Effects of agrochemicals on the radiometric properties of different anti-UV stabilized EVA plastic films. Acta Hortic. 956, 515–522. https://doi.org/10.17660/ActaHortic.2012.956.61.

Serrano-Ruiz Hadaly, Martin-Closas Lluis, Pelacho, Ana M. Biodegradable plastic mulches: impact on the agricultural biotic environment, Sci. Total Environ., Volume 750, 2021, paper n 141228,doi:https://doi.org/10.1016/j.scitotenv.2020.141228.

Sintim Henry Y.,. Bary Andy I, Hayes Douglas G., Wadsworth Larry C., Anunciado Marife B., English Marie E., Bandopadhyay Sreejata, Schaeffer Sean M., DeBruyn Jennifer M., Miles Carol A., Reganold John P., Flury Markus, In situ degradation of biodegradable plastic mulch films in compost and agricultural soils, Sci. Total Environ., Volume 727, 2020, paper n 138668, doi:https://doi.org/10.1016/j.scitotenv.2020.138668.

Tavares, Lara, Ito, Nathalie, Salvadori, Maria, Santos, Demetrio, Rosa, D., 2018. PBAT/Kraft lignin blend in flexible laminated food packaging: peeling resistance and thermal degradability. Polym. Test. 67 https://doi.org/10.1016/j.polymertesting.2018.03.004.

Tosin Maurizio, Barbale Marco, Chinaglia Selene, Degli-Innocenti Francesco. Disintegration and mineralization of mulch films and leaf litter in soil, Polym. Degrad. Stab., Volume 179, 2020, paper n 109309, doi:https://doi.org/10.1016/j.polymdegradstab. 2020.109309.

Touchaleaume, F., Angellier-Coussy, H., César, G., et al., 2018. How performance and fate of biodegradable mulch films are impacted by field ageing. J. Polym. Environ. 26, 2588–2600. https://doi.org/10.1007/s10924-017-1154-7.

Venkatesan, Raja, Rajeswari, Natesan, 2016. ZnO/PBAT nanocomposite films: investigation on the mechanical and biological activity for food packaging. Polym. Adv. Technol. 28 https://doi.org/10.1002/pat.3847.

Villegas, C., Martínez, S., Torres, A., Rojas, A., Araya, R., Guarda, A., Galotto, M.J., 2023. Processing, characterization and disintegration properties of biopolymers based on mater-bi® and Ellagic acid/chitosan coating. Polymers 15, 1548. https://doi.org/10.3390/polym15061548.

Vox, G., Schettini, E., 2007. Evaluation of the radiometric properties of starch-based biodegradable films for crop protection. Polym. Test. 26 (5), 639–651. https://doi.org/10.1016/j.polymertesting.2007.03.010.

Vox, G., Schettini, E., Scarascia-Mugnozza, G., 2005. Radiometric properties of biodegradable films for horticultural protected cultivation. Acta Hortic. 691, 575–582. https://doi.org/10.17660/ActaHortic.2005.691.69.

Wang, J.-M., Wang, H., Chen, E.-C., Chen, Y.-J., Wu, T.-M., 2020. Enhanced Photodegradation stability in poly(butylene adipate-co-terephthalate) composites using organically modified layered zinc Phenylphosphonate. Polymers 12, 1968. https://doi.org/10.3390/polym12091968.

Xiao, H., Lu, W., Yeh, J.-T., 2009. Crystallization behavior of fully biodegradable poly (lactic acid)/poly(butylene adipate-*co*-terephthalate) blends. J. Appl. Polym. Sci. 112, 3754–3763. https://doi.org/10.1002/app.29800.

Yu, Jie, Paterson, Nigel, Millan, Marcos, 2019. The primary products of cellulose pyrolysis in the absence of extraparticle reactions. Fuel 237, 911–915. https://doi.org/10.1016/j.fuel.2018.10.059.

Zhang, Xiaolei, Yang, Weihong, Dong, Changqing, 2013. Levoglucosan formation mechanisms during cellulose pyrolysis. J. Anal. Appl. Pyrolysis 104, 19–27. https://doi.org/10.1016/j.jaap.2013.09.015.

Zhang Yu, Ma Jun, Song Ya-Qiong, Li Gang, O'Connor Patrick. Stronger deterministic processes shape the plastisphere microbiota of biodegradable microplastics compared to non-biodegradable microplastics in farmland soil. Appl. Soil Ecol., Volume 196, 2024, paper n 105312, doi:https://doi.org/10.1016/j.apsoil.2024.105312.

Zhou JieJia RongPlaceholder TextPlaceholder Text, Brown Robert W., Yang Yadong, Zeng Zhaohai, Jones Davey L., Zang Huadong, The long-term uncertainty of biodegradable mulch film residues and associated microplastics pollution on plant-soil health, J. Hazard. Mater., Volume 442, 2023, paper n 130055, doi:https://doi.org/10.1016/j.jhazmat.2022.130055.